Journal of Materials Chemistry C

Accepted Manuscript

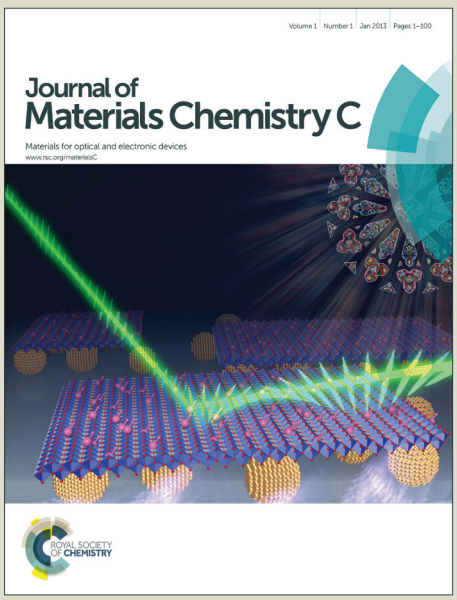

ROYAL SOCIETY OF CHEMISTRY

www.rsc.org/materialsC

Journal of
Materials Chemistry C

RSCPublishing

Fluorenylethynylpyrene Derivatives with Strong Two-Photon Absorption: Influence of Substituents on Optical Properties

C. Lavanya Devi,[a,b] K. Yesudas,[b] Nikolay S. Makarov,[c,d] V. Jayathirtha Rao*,[a,e] K. Bhanuprakash*,[b,e] and Joseph W. Perry*[c]

Cite this: DOI: 10.1039/xoxxooooox

Received ooth January 2012,
Accepted ooth January 2012

DOI: 10.1039/xoxxooooox

www.rsc.org/

The one- and two-photon absorption properties of five newly synthesized pyrene-based chromophores with donor–π–acceptor, donor–π–acceptor–π–donor and acceptor–π–donor–π–acceptor structural motif using mono-, di- and tetra-branched fluorenyl groups linked to pyrene through acetylene π-bridge are systematically studied both experimentally and theoretically. Analysis of the photophysical properties of the materials has been performed to derive structure–property relationships and to formulate guidelines for both spectral tuning and enhancement of molecular two-photon absorption cross-sections in the near-infrared spectral range. The influence of donor/acceptor strength, π-conjugation length, and molecular symmetry on the cross-sections of these new molecules have been studied. These dyes have strong fluorescence quantum yields with good two-photon cross-sections ranging between 250-2500 GM. All of the tetra-substituted chromophores showed relatively strong two-photon absorption in the NIR region with cross-sections in the range of 1500-2500 GM at excitation wavelengths between 700 and 900 nm. Cross-sections as high as 9000 GM can be accessed at shorter wavelengths. The calculated two-photon absorption cross-section values and trends are in good agreement with the experimental results. It was found that the presence of donor or acceptor groups increases the 2PA cross-sections relative to molecules with simple aryl substituents. Increasing the donor strength is conducive to attain large two-photon cross-sections. Moreover, the combination of large two-photon absorption cross-sections and high fluorescence quantum yields make these dyes good two-photon chromophores for a variety of applications.

1. Introduction

Development of organic materials with high two-photon absorption (2PA)[1-9] cross-sections (δ) has attracted great interest in the past decade due to various potential applications in photonics and optoelectronics, such as three-dimensional optical data storage,[10, 11] photochromic switches,[12] fluorescence imaging,[13] multi-photon fabrication,[14] two-photon optical power limiting,[15, 16] and photodynamic therapy,[17, 18] among others. Fluorescent chromophores with large δ are of paramount importance in two-photon fluorescence imaging of biological samples, as they have the advantages of reducing photo-induced damage,[19] increasing penetration depth,[20, 21] enhancing imaging resolution of turbid samples,[19, 20] and diminishing cellular auto-fluorescence background. Various design strategies have been employed for the synthesis of organic molecules with large δ. Accordingly, a wide array of dipolar, quadrupolar, octupolar and multi-branched chromophores have been designed and synthesized to achieve larger δ.[22-27] The prominent and widely studied models, among others, include π-conjugated molecular skeletons with D–π–A,[28-32] D–π–D,[33-37] D–π–A–π–D,[26, 38-42] A–π–A[43] type of architectures, and octupolar type tri-branched chromophores such as A_3-(D-core)[44] and D_3-(A-core)[45] (D = donor and A = acceptor). Analysis of the structure-property relationships in these systems reveal that the δ increases with increasing donor/acceptor strength, conjugation length, and planarity of the π-center.[43, 46] Also, it has been pointed out that extended π-electron conjugation is crucial for achieving large δ. In addition, a significant increase in δ has been discovered in the multi-branched structures, indicating a cooperative enhancement.[44,45]

These general structure-property relationships have prompted us to design and synthesize a series of novel 2PA chromophores containing multi-branched structural motifs based on pyrene core,[47, 48] which displays enhanced δ and fluorescence quantum yields as required for bioimaging applications by taking advantage from tailor-made fluorophores combining high fluorescence quantum yield (Φ). Pyrene is chosen as the core of the chromophore because of its excellent photoluminescence efficiency, planarity and delocalized π-conjugated structure. Moreover, π-extended pyrene derivatives typically have red-shifted fluorescence and enhanced quantum yields compared to the parent pyrene.[49-53] The π-extension of the pyrene core is obtained by employing fluorenyl groups which have been widely used in molecular 2PA research because of its utility in extending the conjugation length which is facilitated by its planar structure.[9] Fluorene substituents are also interesting due to the facile substitution at the C_9 site, which is useful in improving solubility and processability, as well as controlling intermolecular interactions to prevent excimer formation in the excited state.[54, 55] Although the double bond (C=C) is an excellent conjugation bridge, it can readily undergo *cis-trans*-photoisomerization,[43, 56] which may hamper the fluorescence efficiency and the lifetime of the materials. Therefore, we employed the triple bond (C≡C) as a conjugation bridge to improve the photostability.[23, 26, 57-62] Acetylene has been widely employed for efficient linking of π-conjugated units for extending π-conjugation. With the development of Sonogashira coupling reactions, π-conjugated materials involving acetylene linkers are readily prepared.[63-65] Hence, synthesis and systematic study of such derivatives with high 2PA brightness, due to a large product of δ and the fluorescence quantum efficiency, Φ, would be useful for biological imaging applications.

In this work, we report the synthesis and characterization of a series of five novel 2PA chromophores based on the pyrene core: 1-((9,9-dibutyl-9*H*-fluoren-2-yl)ethynyl)pyrene (**PMF**), 1,6-bis((9,9-dibutyl-9*H*-fluoren-2-yl)ethynyl)pyrene (**PDF**), 1,3,6,8-tetrakis((9,9-dibutyl-9*H*-fluoren-2-yl)ethynyl)pyrene (**PTF**), 1,3,6,8-tetrakis ((9,9-dibutyl-7-(9*H*-carbazol-9-yl)-9*H*-fluoren-2-yl)ethynyl)pyrene (**PTC**) and 1,3,6,8-tetrakis((9,9-dibutyl-7-nitro-9*H*-fluoren-2-

yl)ethynyl)pyrene (**PTN**) (Scheme 1). The donor/acceptor character of the fluorenyl groups is tuned by the substituents at the 7-position. The substituents include -H (unbiased), -carbazole (electron-donating) and -NO_2 (electron-accepting) groups. As the pyrene core is polarizable but not polar; its electronic properties will depend on the nature of the substituents. Thus, if an electron-donating group is present on the fluorene group, the pyrene core acts as an acceptor and if an electron acceptor group is present on the fluorene, pyrene core acts as a donor. Therefore, the compounds synthesized here are designated as D–π–A (**PMF**), D–π–A–π–D (**PDF**, **PTF** and **PTC**) and A–π–D–π–A (**PTN**) respectively.

The main theme of this work is to elucidate both experimentally and theoretically the structure-property relationships for one-photon absorption (1PA) and 2PA of these dyes by considering structural modifications such as (i) the effect of number of branches on the pyrene core, i.e. mono-, di- and tetra-branched structures (ii) symmetry of the structure, (iii) impact of strength of donor or acceptor groups on the pyrene core and (iv) increasing the two-photon cross-sections and two-photon brightness.

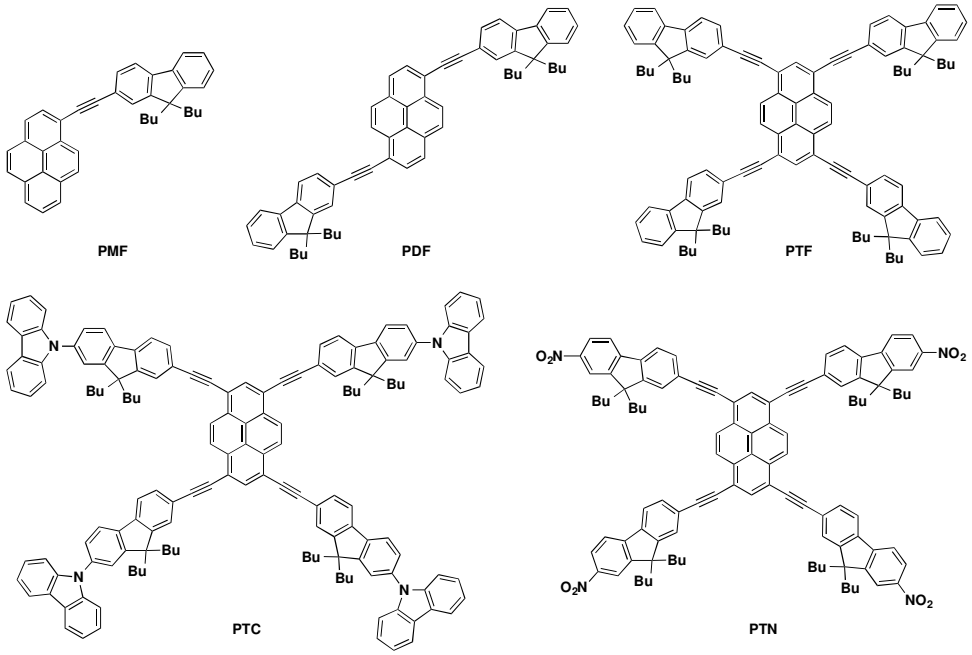

Scheme 1 Chemical structures of the fluorenylethynylpyrene derivatives.

2. Experimental section

2. 1. *Materials and instruments*

All the reagents are of Analytical Reagent grade and used without further purification except for DMF, which is distilled from molecular sieves, BaO and CaH_2. ^{1}H-NMR spectra were recorded on a Bruker Avance (300 MHz) spectrometer and ^{13}C-NMR spectra on a Bruker Avance (75 MHz) spectrometer in $CDCl_3$ with TMS as internal standard in both cases. Mass spectra were obtained by electron ionization technique using VG70-70H mass spectrometer and also MALDI-TOFTOF with an Applied Biosystems, USA 4800 spectrometer using α-cyano-4-hydroxycinnamic acid as the matrix. UV-Visible absorption spectra were measured on a Jasco V-550 spectrophotometer. Steady state fluorescence spectra were recorded using a Spex model Fluorolog-3 spectrofluorometer. The fluorescence quantum yields (Φ) were estimated by using 9,10-diphenylanthracene (DPA) as the standard.[66] Perkin-Elmer Spectrum BX spectrophotometer was used to obtain IR spectra of the sensitizer at a resolution of 4 cm^{-1}, where all the samples were pressed into KBr pellets. TGA was performed using TGA/SDTA 851e (METLER TOLEDO) under nitrogen. Elemental analysis was performed using Vario-EL elemental analyzer.

2. 2. *Two-photon and excited-state absorption measurements techniques*

The excited state absorption (ESA) was measured using Ultrafast Systems Helios nonlinear spectrometer as was described earlier.[60] The excited state molar absorptivities were estimated based on the comparison of the ESA bleach to the 1PA molar absorptivity[67] and also based on the measured excited-state absorbance and an excited-state population distribution along the beam path through the cell.[60] 2PA was measured using two-arm two-photon excited fluorescence spectrometer as described elsewhere.[68] To avoid any possible solvent-initiated photochemistry the spectra were measured in toluene using coumarin 485 and rhodamine 6G dissolved in methanol as reference standards.[69] The δ were measured at excitation wavelength of 570 nm for **PMF** and **PDF**, and at 650 nm for **PTF**, **PTC**, and **PTN** relative to coumarin 485.

2. 3. *Computational details*

To gain an insight about the nature of 1PA and 2PA transitions, first principles calculations based on the density functional theory (DFT) were performed. The gas phase geometry optimizations of all the compounds in the ground state were carried out at hybrid B3LYP level with a $C_s/C_2/C_{2h}$ symmetry constraint respectively for **PMF/PTC/PDF**, **PTF** and **PTN** and by replacing the butyl solubilizing chains with methyl groups. The vibrational frequency

analysis was carried out to ensure that the obtained geometries represent minima on the potential energy surface. The time dependent (TD)-DFT has been applied to calculate the lowest 20 1PA transitions and associated state- and transition-dipole moments (μ_g, μ_e and μ_{ge}). All these calculations have been performed using the Gaussian 09 program.[70] The transition dipole moments between the excited states ($\mu_{ee'}$) and δ are calculated by use of the response theory implemented in the DALTON2011 program.[71] All the excited state properties have been calculated with the range separated functional CAM-B3LYP.[72] A 6-31G** basis set has been employed in all the calculations.

The 2PA transition matrix elements ($S_{\alpha\beta}$) are evaluated using the sum-over-states approach truncated to the essential states model (equation 1) with the quantities obtained above:

$$S_{\alpha,\beta} = \left[\frac{\langle g|\mu_\alpha|i\rangle\langle i|\mu_\beta|f\rangle}{\omega_i - \omega_f/2} + \frac{\langle g|\mu_\beta|i\rangle\langle i|\mu_\alpha|f\rangle}{\omega_i - \omega_f/2} \right] \quad (1)$$

where μ is the dipole operator in the directions $\alpha, \beta \in (x, y, z)$, ω_i and ω_f are the transition energies for the intermediate state $|i\rangle$ and the final two-photon state $|f\rangle$ respectively. The microscopic 2PA transition probability (δ_{TP}) can then be obtained by the orientational averaging over the transition matrix (S) using equation 2:

$$\delta_{TP} = F\delta_F + G\delta_G + H\delta_H$$
$$\text{where } \delta_F = \sum_{\alpha,\beta} S_{\alpha\alpha}S_{\beta\beta} \quad \delta_G = \sum_{\alpha,\beta} S_{\alpha\beta}S_{\alpha\beta} \quad \delta_H = \sum_{\alpha,\beta} S_{\alpha\beta}S_{\alpha\beta} \quad (2)$$

Where $F = G = H = 2$ for a linearly polarized light. Finally, the relation between macroscopic cross-section (δ in Goppert-Mayer units, 10^{-50} cm^4 s/photon) and microscopic transition probability (δ_{TP} in atomic units) is given by equation 3:

$$\delta = \frac{4\pi^2 \alpha a_0^5 \omega_i^2}{15c\Gamma} \delta_{TP} = 2.1717 \times 10^{-50} \omega_i^2 \delta_{TP} \quad (3)$$

where, α is the fine structure constant (7.297×10^{-3}), c is the velocity of light (3×10^{10} cm/sec) and a_0 is the Bohr's first radius (0.529×10^{-8} cm), ω is the angular frequency of the exciting photon in cm^{-1}, Γ is the state damping factor which is fixed at 0.1 eV in our calculations (although in real solutions it varies from molecule to molecule).

3. Synthesis and characterization

3.1. General procedure for the preparation of key intermediates:

Bromopyrenes *viz.*, 1-bromopyrene[51, 73] (**1**), 1,6-dibromopyrene[74] (**2**), and 1,3,6,8-tetrabromopyrene[75] (**3**) are synthesized by the bromination of pyrene as reported. The synthesis of key intermediates, substituted ethynylfluorenes (compounds **7, 10, 16**) were shown in Scheme 2. 2-Bromofluorene (**4**) was alkylated with *n*-BuBr to get 2-bromo-9,9-dibutylfluorene (**5**)[76] followed by nitration to obtain 2-Bromo-9,9-dibutyl-7-nitro-9*H*-fluorene (**8**). Fluorene (**11**) was brominated in the presence of Fe catalyst to get 2,7-dibromofluorene (**12**).[77] Compound **12** was alkylated using *n*-BuBr in presence of base *t*-BuOK to form 2,7-dibromo-9,9-dibutylfluorene (**13**). A classic Ullmann coupling was used to form C–N bond by reacting carbazole and 2,7-dibromo-9, 9-dibutylfluorene (**13**) in presence of CuI/proline catalyst[78] to get 9-(7-bromo-9,9-dibutyl-9*H*-fluoren-2-yl)-9*H*-carbazole (**14**).

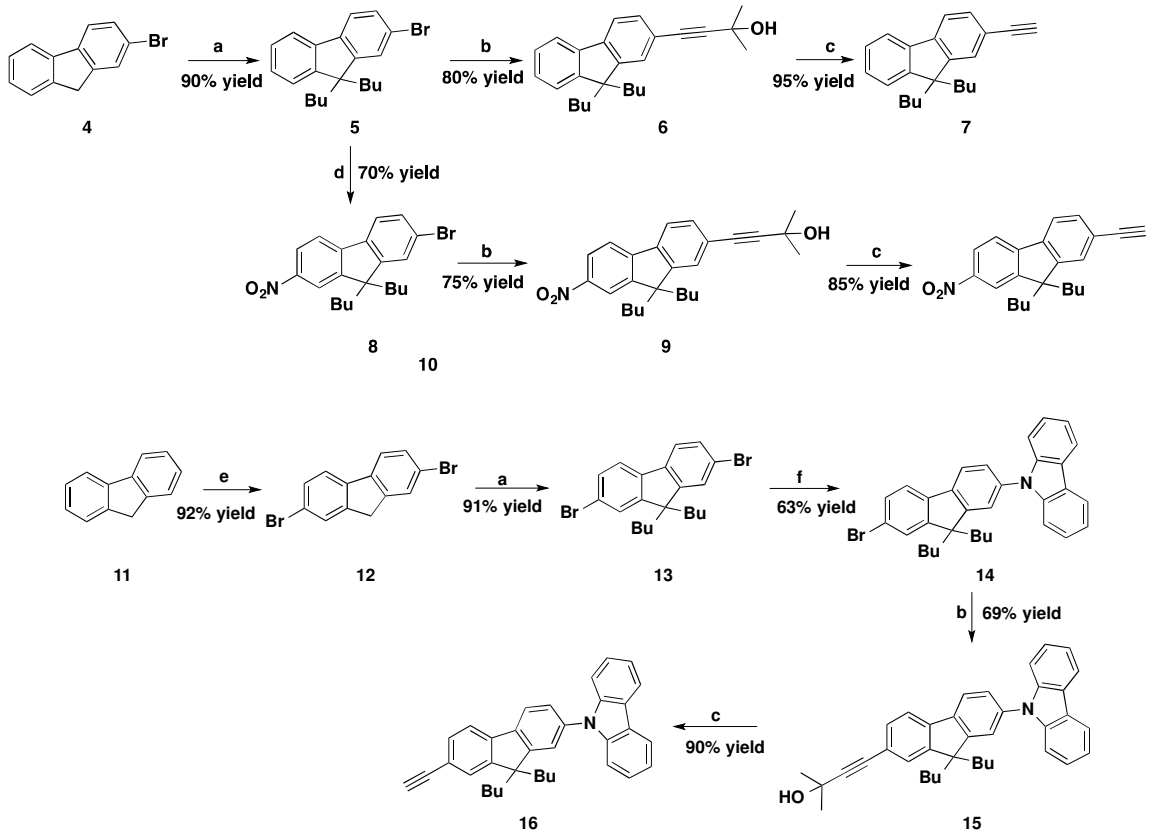

Scheme 2 Synthesis of substituted ethynylfluorenes, where Bu= *n*-butyl.

Reagents and conditions: (a) *t*BuOK (3 eq.), *n*-BuBr (2.5 eq.), 0 °C-rt, 8 h. (b) 2-methyl-3-butyn-2-ol (2 eq.), 2 mol% $Pd(PPh_3)_2Cl_2$, 2 mol% CuI, toluene/Et_3N, 70 °C, 12 h. (c) KOH, *i*PrOH, reflux, 3 h (d) HNO_3, AcOH, reflux, 45 min. (e) Br_2 (2.1 eq), Fe (0.015 eq.), 5 °C, 2 h. (f) 20 mol% CuI, 20 mol% L-proline, carbazole (1 eq.), 15 (1.5 eq.), 2.5 eq. K_2CO_3, DMF, reflux, 24 h.

Compounds **5**, **8** and **14** were coupled with 2-methyl-3-butyn-2-ol by applying Sonogashira reaction[64, 65] to form alkynol compounds 4-(9,9-Dibutyl-9*H*-fluoren-2-yl)-2-methylbut-3-yn-2-ol **(6),** 4-(9,9-Dibutyl-7-nitro-9*H*-fluoren-2-yl)-2-methylbut-3-yn-2-ol **(9)** and 4-(9,9-Dibutyl-7-(9*H*-carbazol-9-yl)-9*H*-fluoren-2-yl)-2-methylbut-3-yn-2-ol **(15)**, which are then de-protected using KOH in *i*PrOH to obtain the alkynyl intermediates viz., 9,9-dibutyl-2-ethynyl-9*H*-fluorene (**7**), 9,9-dibutyl-2-ethynyl-7-nitro-9*H*-fluorene (**10**) and 9-(7-ethynyl-9,9-dibutyl-9*H*-fluoren-2-yl)-9*H*-carbazole (**16**).

2-Bromo-9,9-dibutyl-9*H*-fluorene (5): To a stirred solution of **4** (4.9 g, 20 mmol) in 50 mL THF under nitrogen was added *t*BuOK (6.73 g, 60 mmol) in 50 mL THF slowly at 0 °C. After 1 h *n*-BuBr (6.85 g, 50 mmol) was added to the reaction mixture and stirred at room temperature for 8 h. The reaction mixture was filtered to remove the formed KBr and the organic layer was concentrated under reduced pressure. The oily residue was purified by flash column chromatography (silica gel, hexane) to obtain colourless oily liquid, which gives white crystals on standing (5.26 g, 90% yield). ^{1}H NMR ($CDCl_3$, 300 MHz): δ 0.51-0.64 (m, 4 H), 0.67-0.70 (t, *J* = 7.49 Hz, 6H), 1.04-1.11 (m, 4H), 1.87-1.98 (m, 4H), 7.27-7.29 (s, 3H), 7.40-7.43 (d, *J* = 6.42 Hz, 2H), 7.50-7.53 (d, *J* = 8.56 Hz, 1H), 7.60 - 7.63 (d, *J* = 4.28 Hz, 1H). IR (KBr) in cm^{-1}: 736, 821, 1443, 2857,2925, 2953, 3023. MS-EI: m/z 358 $[M+2]^+$

4-(9,9-Dibutyl-9*H*-fluoren-2-yl)-2-methylbut-3-yn-2-ol (6): A solution of **5** (14 mmol, 5 g), 2-methylbut-3-yn-2-ol (28 mmol, 2.35 g) and $Pd(PPh_3)_2Cl_2$ (0.28 mmol, 197 mg) in 20 mL of toluene/Et_3N (5/1) was degassed with nitrogen for 30 min. Then CuI (0.28 mmol, 53 mg) was added at once and deaeration was continued for 10 min. Thereafter, stirring was continued at 70 °C for 12 h. The solvent was removed under reduced pressure and the reaction mixture diluted with ethyl acetate. The resulting solution was filtered through a pad of celite. The filtrate was concentrated and the crude product was purified by column chromatography (silica gel, hexane 98%, ethyl acetate 2%) to afford a white solid (4.03 g, 80% yield). ^{1}H NMR ($CDCl_3$, 300 MHz): δ 0.46-0.62 (m, 4 H), 0.64-0.72 (t, *J* = 7.55 Hz, 6H), 1.01-1.14 (m, 4 H), 1.64 (s, 6H), 1.89-1.99 (q, 4H, *J* = 8.31), 7.26-7.30 (m, 3H), 7.32 (s, 1H), 7.33-7.37 (dd, *J* = 8.31, *J* = 1.51 Hz, 2H), 7.57-7.60 (d, *J* = 7.55 Hz, 1H), 7.61-7.65 (m, 1H). ^{13}C NMR ($CDCl_3$, 75 MHz): δ 13.91, 23.07, 25.86, 31.65, 40.29, 54.96, 65.57, 93.73, 96.18, 119.48, 120.01, 121.05, 122.68, 125.79, 126.90, 127.48, 130.70, 140.36, 150.76. IR (KBr) in cm^{-1}: 736,1160, 1455, 2859, 2927, 2956, 3062, 3330. MS-EI: m/z 360 $[M]^+$

9,9-Dibutyl-2-ethynyl-9*H*-fluorene (7): A mixture of **6** (2.75 g, 7.64 mmol) and KOH (2.14 g, 38 mmol) in 60 mL of *i*PrOH was heated at reflux under nitrogen with vigorous stirring for 3h. The solvent was then removed and the crude product was purified by column chromatography (silica gel, hexane) to afford a white solid (2.2 g, 95 % yield). ^{1}H NMR ($CDCl_3$, 300 MHz): δ 0.49-0.62 (m, 4 H), 0.63-0.73 (t, *J* = 7.55 Hz, 6H), 1.01-1.14 (m, 4 H), 1.89-1.99 (t, 4H, *J* = 8.31), 3.03 (s, 1H), 7.26-7.32 (m, 3H), 7.39-7.46 (m, 2H), 7.59-7.66 (m, 2H). ^{13}C NMR ($CDCl_3$, 75 MHz): δ 13.86, 23.09, 25.93, 40.19, 55.08, 76.98, 84.80, 119.62, 120.12, 122.95, 126.56, 126.94, 127.70, 131.16, 140.29, 141.98, 150.72, 151.07. IR (KBr) in cm^{-1}: 740, 1455, 2104, 2858, 2927, 2957, 3062, 3302. MS-EI: m/z 302 $[M]^+$

2-Bromo-9,9-dibutyl-7-nitro-9*H*-fluorene (8): Conc. HNO_3 (5.4 mL) was added to **5** (5 g, 14 mmol) in acetic acid (50 mL). The mixture was heated to boiling over 30 min. and kept at this temperature for 15 min. The yellow solid which was separated from the cold solution was filtered and recrystallized from ethanol to afford pale yellow solid (3.94 g, 70% yield). ^{1}H NMR ($CDCl_3$, 300 MHz): δ 0.48-0.64 (m, 4 H), 0.66-0.75 (t, *J* = 7.37 Hz, 6H), 1.04-1.18 (m, 4 H), 1.92-2.11 (m, 4H), 7.5 (s, 1H), 7.53-7.54 (d, *J* = 1.70 Hz, 1H), 7.61-7.64 (d, *J* = 7.93 Hz, 1H), 7.74-7.77 (d, *J* = 8.31 Hz, 1H), 8.15-8.16 (d, *J* = 1.89 Hz, 1H), 8.24-8.27 (dd, *J* = 8.31, *J* = 1.89 Hz, 1H). IR (KBr) in cm^{-1}: 736, 821,1443, 2857, 2925, 2953, 3023. MS-EI: m/z 403 $[M+2]^+$

4-(9,9-Dibutyl-7-nitro-9*H*-fluoren-2-yl)-2-methylbut-3-yn-2-ol (9): A solution of **8** (9.7 mmol, 3.9 g), 2-methylbut-3-yn-2-ol (19.4 mmol, 1.63 g) and $Pd(PPh_3)_2Cl_2$ (0.194 mmol, 136 mg) in 20 mL of toluene/Et_3N (5/1) was degassed with nitrogen for 30 min. Then CuI (0.194 mmol, 37 mg) was added at once and deaeration was continued for 10 min. Thereafter, stirring was continued at 70 °C for 12 h. The solvent was removed under reduced pressure and the reaction mixture diluted with ethyl acetate. The resulting solution was filtered through a pad of celite. The filtrate was concentrated and the crude product was purified by column chromatography (silica gel, hexane 98%, ethyl acetate 2%) to afford a pale yellow solid (2.96 g, 75% yield). ^{1}H NMR ($CDCl_3$, 300 MHz): δ 0.47-0.62 (m, 4 H), 0.66-0.72 (t, *J* = 7.10 Hz, 6H), 1.06-1.15 (m, 4 H), 1.64 (s, 6H), 1.96-2.08 (m, 4H), 7.38 (s, 1H), 7.41-7.45 (dd, *J* = 7.99, *J* = 1.78 Hz, 1H), 7.68-7.71 (d, *J* = 7.99 Hz, 1H), 7.74-7.77 (d, *J* = 8.88 Hz, 1H), 8.15-8.16 (d, *J* = 2.66 Hz, 1H), 8.24-8.27 (dd, *J* = 8.88, *J* = 2.66 Hz, 1H). ^{13}C NMR ($CDCl_3$, 75 MHz): δ 13.75, 22.89, 25.84, 31.48, 39.87, 55.65, 65.74, 82.49, 95.01, 118.22, 120.09, 121.02, 123.35, 126.26, 131.13, 138.75, 146.74, 147.30, 152.14, 152.21. IR (KBr) in cm^{-1}: 738, 825, 1131, 1338, 1517, 1600, 2862, 2927, 2953, 3398.MS-EI: m/z 405 $[M]^+$

9,9-Dibutyl-2-ethynyl-7-nitro-9*H*-fluorene (10): A mixture of **9** (2.75 g, 6.76 mmol) and KOH (1.89 g, 34 mmol) in 50 mL of *i*PrOH was heated at reflux under nitrogen with vigorous stirring for 3 h. The solvent was then removed and the crude product was purified by column chromatography (silica gel, hexane) to afford a pale yellow solid (2.0 g, 85 % yield). ^{1}H NMR ($CDCl_3$, 300 MHz): δ 0.46-0.63 (m, 4 H), 0.67-0.72 (t, *J* = 7.18 Hz, 6H), 1.04-1.16 (m, 4 H), 1.95-2.10 (m, 4H), 3.14 (s, 1H), 7.47 (s, 1H), 7.50-7.53 (d, *J* = 7.93 Hz, 1H), 7.70-7.73 (d, *J* = 7.74 Hz, 1H), 7.76-7.79 (d, *J* = 8.31 Hz, 1H), 8.16-8.17 (d, *J* = 1.89 Hz, 1H), 8.25-8.27 (dd, *J* = 8.31, *J* = 1.89 Hz, 1H). ^{13}C NMR ($CDCl_3$, 75 MHz): δ 13.85, 22.98, 25.97, 39.90, 55.69, 78.69, 83.99, 118.22, 120.15, 121.05, 122.96, 123.39, 126.70, 130.84, 131.68, 139.24, 146.41, 147.62, 152.20. IR (KBr) in cm^{-1}: 826, 1340, 1518, 1588, 2860, 2927, 2955, 3280. MS-EI: m/z 347 $[M]^+$

2,7-Dibromo-9*H*-fluorene (12): Bromine (10.1 g, 63 mmol) in 20 mL of chloroform was added drop wise into a suspension solution containing **11** (5.0 g, 30.8 mmol), iron powder (26 mg, 0.46 mmol) in a catalytic amount and 50 mL of chloroform. The flask was cooled by ice water, and the temperature was controlled under 5 °C. The reaction was allowed to stand for 2 h. The product was filtered and recrystallized with chloroform, to afford white crystals (8.95 g, 92% yield). ^{1}H NMR ($CDCl_3$, 300 MHz): δ 3.84 (s, 2H), 7.44-7.49 (d, *J* = 8.31 Hz 2H), 7.53-7.59 (d, *J* = 8.31 Hz, 2H), 7.63 (s, 2H). IR (KBr) in cm^{-1}: 808, 1395, 2917, 3047. MS-EI: m/z 324 $[M+2]^+$

2,7-Dibromo-9,9-dibutyl-9*H*-fluorene (13): To a stirred solution of **12** (8 g, 24.8 mmol) in 100 mL THF under nitrogen was added *t*BuOK (12.83 g, 74.5 mmol) in 100 mL THF slowly at 0 °C. After 1 h *n*-BuBr (8.53 g, 62.8 mmol) was added to the reaction mixture and stirred at room temperature for 8 h. The reaction mixture was filtered and the organic layer was concentrated under reduced pressure. The oily residue was purified by flash column chromatography (silica gel, hexane) to afford white solid (9.85 g, 91% yield). ^{1}H NMR ($CDCl_3$, 300 MHz): δ 0.52-0.62 (m, 4 H), 0.69-0.73 (t, *J* = 7.55 Hz, 6H), 1.04-1.17 (m, 4 H), 1.88-1.94 (m, 4H), 7.39-7.45 (m, 4H), 7.48-7.51 (d, *J* = 7.93 Hz, 2H). **IR** (KBr) in cm^{-1}: 810, 1449, 2859, 2924, 2953, 3059. MS-EI: m/z 436 $[M]^+$

9-(7-Bromo-9,9-dibutyl-9*H*-fluoren-2-yl)-9*H*-carbazole (14): A mixture of **13** (6.25 g, 14.3 mmol), carbazole (1.61 g, 9.5 mmol), crushed K_2CO_3 (3.29 g, 23.8 mmol), CuI (363 mg, 1.91 mmol), L-proline (219 mg, 1.9 mmol) were taken in 50 mL of DMF and refluxed under nitrogen atmosphere for 24 h. DMF was removed under reduced pressure. The resulting mixture is then diluted with ethyl acetate and filtered through a small pad of silica gel. The filtrate was concentrated and the residue was purified by column chromatography (silica gel, hexane) to afford white solid (2.9 g, 63 % yield). ^{1}H NMR ($CDCl_3$,300 MHz): δ 0.68-0.79 (m, 10 H), 1.07-1.20 (m, 4 H), 1.91-2.06 (m, 4H), 7.22-7.23 (d, *J* = 2.45 Hz, 1H), 7.26-7.27 (d, *J* = 2.45 Hz, 1H), 7.33-7.40 (m, 4H), 7.48-7.62 (m, 5H), 7.84-7.87 (d, *J* = 7.93 Hz, 1H), 8.10-8.12 (d, *J* = 7.74 Hz, 2H). IR (KBr) in cm^{-1}: 749, 1226, 1452, 1597, 2853, 2922, 2951,3054. MS-EI: m/z 523 $[M+2]^+$

4-(9,9-Dibutyl-7-(9*H*-carbazol-9-yl)-9*H*-fluoren-2-yl)-2-methylbut-3-yn-2-ol (15): A solution of **14** (2 g, 4.2 mmol), 2-methylbut-3-yn-2-ol (698 mg, 8.3 mmol) and $Pd(PPh_3)_2Cl_2$ (58 mg, 0.083 mmol) in 20 mL of toluene/Et_3N (5/1) was degassed with nitrogen for 30 min. Then CuI (16 mg, 0.083 mmol) was added at once and deaeration was continued for 10 min. Then, stirring was continued at 70 °C for 12 h. The solvent was removed under reduced pressure and the reaction mixture diluted with ethylacetate. The resulting solution was filtered through celite. The filterate was concentrated and the crude product was purified by column chromatography (silica gel, hexane 95%, ethyl acetate 5%) to afford a white solid (1.5 g, 69% yield). ^{1}H NMR ($CDCl_3$, 300 MHz): δ 0.66-0.78 (m, 10 H), 1.08-1.21 (m, 4 H), 1.66 (s, 6H), 1.96-2.04 (m, 4H), 7.22-7.23 (d, *J* = 2.27 Hz, 1H), 7.26-7.27 (d, *J* = 2.27 Hz, 1H), 7.33-7.44 (m, 6H), 7.52-7.57 (m, 2H), 7.66-7.69 (d, *J* = 8.31 Hz, 1H), 7.85-7.88 (d, *J* = 7.55 Hz, 1H), 8.09-8.12 (d, *J* = 7.55 Hz, 2H). ^{13}C NMR ($CDCl_3$, 75 MHz): δ 13.84, 22.99, 26.05, 31.58, 40.02, 55.35, 65.77, 82.98, 109.73, 119.72, 119.92, 120.37, 121.12, 121.29, 121.70, 123.39, 125.78, 125.91, 126.14, 130.92, 136.78, 139.59, 140.53, 140.92, 150.96, 152.82. IR (KBr) in cm^{-1}: 749, 1159, 1228, 1454, 1602, 2858, 2926, 3054, 3354. MS-EI: m/z 525 $[M]^+$

9-(9,9-Dibutyl-7-ethynyl-9*H*-fluoren-2-yl)-9*H*-carbazole (16): A mixture of **15** (1 g, 1.9 mmol) and KOH (533 mg, 9.52 mmol) in 30 mL of *i*PrOH was heated at reflux under nitrogen with vigorous stirring for 3 h. The solvent was then removed and the crude product was purified by column chromatography (silica gel, hexane) to afford white solid (0.8 g, 90% yield). ^{1}H NMR ($CDCl_3$, 300 MHz): δ 0.66-0.80 (m, 10 H), 1.07-1.21 (m, 4 H), 1.95-2.04 (m, 4H), 3.08 (s, 1H), 7.21-7.28 (td, *J* = 7.74, *J* = 1.89 Hz, 2H), 7.33-7.42 (m, 4H), 7.46-7.58 (m, 4H), 7.67-7.71 (d, *J* = 7.74 Hz, 1H), 7.85-7.89 (d, *J* = 7.93 Hz, 1H), 8.09-8.13 (d, *J* = 7.74 Hz, 2H).^{13}C NMR ($CDCl_3$, 75 MHz): δ 14.07, 23.16, 26.24, 40.15, 55.44, 77.71, 84.61, 109.72, 119.81, 120.09, 120.49, 121.15, 121.28, 121.79, 132.65, 126.01, 126.56, 131.58, 137.23, 139.50, 140.98, 150.92, 151.91. IR (KBr) in cm^{-1}: 749, 1226, 1451, 1601, 1886,2101, 2855, 2923, 2952, 3053, 3275. MS-EI: m/z 467 $[M]^+$

3.2. General procedure for the synthesis of Pyrene derivatives:

The synthesis of final compounds **PMF, PDF, PTF, PTC**, and **PTN** is outlined in Scheme 3. The bromopyrenes **1**, **2** and **3** (1 eq) are coupled with **7** in 1.2, 2.4 and 4.5 equivalents respectively by standard Sonogashira coupling reaction in toluene to give **PMF** (87 %), **PDF** (58.5 %), and **PTF** (58.35 %) in moderate to good yields. Similarly, **3** is coupled with **16** and **10** respectively to give **PTC** (47 %) and **PTN** (20 %). The final compounds were fully characterized by all spectroscopic methods. Moreover the compounds are thermally stable, and the initial decomposition temperatures are found to be 300 °C for **PMF**, 410 °C for **PDF**, 400-420 °C for **PTF, PTC**, and 320 °C for **PTN**.

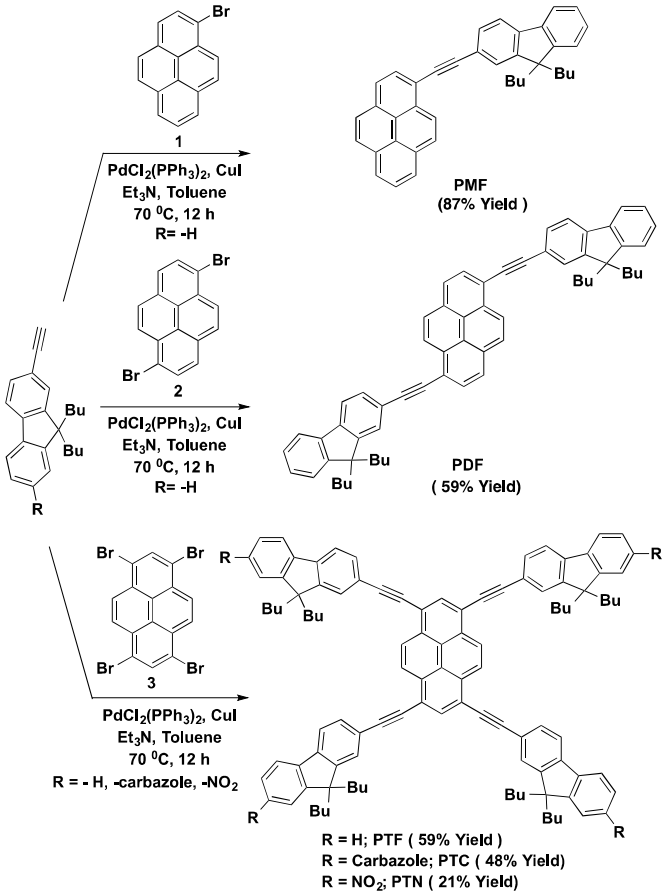

Scheme 3 Synthesis of the fluorenylethynylpyrene derivatives.

1-((9,9-Dibutyl-9*H*-fluoren-2-yl)ethynyl)pyrene (PMF): Compound **1** (180 mg, 0.64 mmol), $[PdCl_2(PPh_3)_2]$ (9 mg, 0.013 mmol), CuI (2.4 mg, 0.013 mmol), were added to a degassed solution of Et_3N (5 mL) and toluene (10 mL) under nitrogen. Compound **7** (0.271 mg, 0.89 mmol) in toluene (2mL) was added slowly. After the mixture was stirred at 70 °C for 12 h, the solvent was removed under reduced pressure and the reaction mixture diluted with ethyl acetate. The resulting solution was filtered through celite. The filtrate was concentrated and the crude product was purified by column chromatography (silica gel, hexane) to afford a pale green colour solid (280 mg, 87% yield). ^{1}H NMR ($CDCl_3$, 300 MHz): δ 0.46-0.65 (m, 10 H), 0.94-1.09 (m, 4H), 1.88-1.99 (t, *J* = 7.93 Hz, 4H), 7.23-7.29 (m, 3H), 7.56-7.69 (m, 4H), 7.90-8.13 (m,

8H), 8.61-8.67 (d, *J* = 9.25 Hz, 1H). ^{3}C NMR ($CDCl_3$, 75 MHz): δ 13.85, 23.08, 25.93, 40.25,55.13, 88.66, 96.34, 118.01, 119.74, 120.02, 121.02, 121.64, 122.91, 124.37, 124.57, 125.54, 125.58, 125.64, 125.92, 126.22, 126.89, 127.26, 127.55, 128.08, 128.28, 129.60, 130.77, 131.11, 131.16, 131.27, 131.83, 140.44, 141.60, 150.89, 151.05. IR (KBr) in cm^{-}: 739, 841, 1452, 1586, 2856, 2923, 3039. MS-EI: m/z 502 $[M]^+$. Elemental anal. Calc for: C, 93.18: H, 6.82. Found: C, 93.05: H, 6.90. mp: 155-157 °C, Td: 300 °C.

1,6-Bis((9,9-dibutyl-9*H*-fluoren-2-yl)ethynyl)pyrene (PDF): Compound **2** (100mg, 0.28 mmol), $PdCl_2(PPh_3)_2$ (9.7 mg, 0.014 mmol), CuI (2.6 mg, 0.014 mmol), were added to a degassed solution of Et_3N (5 mL) and toluene (10 mL) under nitrogen. Compound **7** (0.2 g, 0.66 mmol) in toluene (2 mL) was added slowly, and the reaction mixture was stirred at 70 °C for 12 h. After cooling to room temperature, a yellow precipitate is formed. The solution was filtered and the precipitate was washed with ethyl acetate. The product was further purified by slow precipitation from a $CHCl_3$/MeOH mixture to afford a yellow colour solid (0.130 g, 59 % yield). ^{1}H NMR ($CDCl_3$, 300 MHz): δ 0.51-0.77 (m, 20 H), 1.05-1.21 (m, 8H), 1.95-2.10 (t, *J* = 7.74 Hz, 8H), 7.27-7.37 (m, 6H), 7.57- 7.77 (m, 8H), 8.12-8.28 (m, 6H), 8.69-8.76 (d, *J* = 9.07 Hz, 2H). ^{13}C NMR ($CDCl_3$, 75 MHz): δ 13.83, 23.08, 25.96, 40.25, 55.16, 88.58, 96.78, 118.71, 119.76, 120.06, 121.56, 122.94, 124.36, 125.19, 125.95, 126.36, 126.92, 127.60, 128.15, 129.99, 130.82, 131.14, 132.02, 140.43, 141.72, 150.94, 151.08. IR (KBr) in cm^{-1}: 737, 838, 1066, 1454, 1649, 2859, 2925, 3045. MALDI-TOF-MS: (*m*/*z*) 802.43 (100%) $[M^+]$. Elemental anal. Calc for: C, 92.72: H, 7.28. Found: C, 92.59: H, 7.39. mp: 259-261 °C, Td: 410 °C.

1,3,6,8-Tetrakis((9,9-dibutyl-9*H*-fluoren-2-yl)ethynyl)pyrene (PTF): Compound **3** (100 mg, 0.2 mmol), $[PdCl_2(PPh_3)_2]$ (14 mg, 0.02 mmol), CuI (1.9 mg, 0.01 mmol), were added to a degassed solution of Et_3N (5 mL) and toluene (10 mL) under nitrogen. Compound **7** (0.272 g, 0.9 mmol) in toluene (2 mL) was added slowly. After the mixture was stirred at 70 °C for 12 h, the solvent was removed under reduced pressure and the reaction mixture diluted with ethyl acetate. The resulting solution was filtered through a pad of celite. The filtrate was concentrated and the crude product was purified by column chromatography (silica gel, hexane). The residue was reprecipitated from $CHCl_3$-MeOH (158 mg, 59% yield) to afford orange colour solid. ^{1}H NMR ($CDCl_3$, 300 MHz): δ 0.54-0.78 (m, 40 H), 1.08-1.22 (q, *J* = 7.18 Hz, 16H), 1.99-2.11 (m, 16H), 7.28-7.39 (m, 12H), 7.63- 7.67 (s, 4H), 7.68-7.79 (m, 12H), 8.58 (s, 2H), 8.88 (s, 4H). ^{13}C NMR ($CDCl_3$, 75 MHz): δ 13.87, 23.10, 25.96, 40.27, 55.17, 87.88, 97.35, 119.17, 119.83, 120.10, 121.34, 122.94, 124.27, 126.04, 126.94, 127.66, 130.88, 131.70, 133.82, 140.38, 141.88, 150.95, 151.09. IR (KBr) in cm^{-1}: 737, 827, 1062, 1455, 1599, 2859, 2926, 2955, 3058. MALDI-TOF-MS: (*m*/*z*) 1403.8 (100 %) $[M]^+$. Elemental anal. Calc for: C, 92.39: H, 7.61. Found: C, 92.37: H, 7.62. mp: 304-306 °C, Td: 402 °C.

1,3,6,8-Tetrakis((9,9-dibutyl-7-(9*H*-carbazol-9-yl)-9*H*-fluoren-2-yl)ethynyl)pyrene (PTC): Compound **3** (180 mg, 0.35 mmol), $PdCl_2(PPh_3)_2$ (24 mg, 0.035mmol), CuI (3.3 mg, 0.017 mmol), were added to a degassed solution of Et_3N (5 mL) and toluene (10 mL) under nitrogen. Compound **16** (0.730 g, 1.56 mmol) in toluene (5 mL) was added slowly. After the mixture was stirred at 70 °C for 12 h, the solvent was removed under reduced pressure and the reaction mixture diluted with ethyl acetate. The resulting solution was filtered through celite. The filtrate was concentrated and the crude product was purified by column chromatography (silica gel, $CHCl_3$-hexane 20/80 v/v) to afford a yellow colour solid (340 mg, 48% yield). ^{1}H NMR ($CDCl_3$, 300 MHz): δ 0.74-0.91 (m, 40 H), 1.13-1.30 (m, 16H), 2.03-2.22 (m,16H), 7.28-7.38 (t, *J* = 6.42 Hz, 8H), 7.40-7.52 (m, 16H), 7.57-7.64 (d, *J* = 5.85 Hz, 8H), 7.76-7.91 (m, 12H), 7.94-8.01 (d, *J* = 8.50 Hz, 4H), 8.15-8.23 (d, *J* = 7.55 Hz, 8H), 8.63 (s, 2H), 8.96 (s, 4H). ^{13}C NMR ($CDCl_3$, 75 MHz): δ 13.93, 23.07, 26.16, 40.14, 55.53, 88.22, 97.26, 109.75, 118.67, 119.20, 119.98, 120.08, 120.42, 121.30, 121.74, 123.42, 124.35, 125.96, 126.17, 127.07, 131.17, 131.83, 133.94, 136.98, 139.55, 140.90, 141.08, 151.31, 152.98, 153.25. IR (KBr) in cm^{-1}: 747, 823, 1225, 1343, 1457, 1599, 2858, 2923, 3048. MALDI-TOF-MS: (*m*/*z*) 2064.04 (100 %) $[M]^+$. Elemental anal. Calc for: C, 90.74: H, 6.54: N, 2.71. Found: C, 90.71: H, 6.53: N, 2.69. mp: 273-275 °C, Td: 415 °C.

1,3,6,8-Tetrakis((9,9-dibutyl-7-nitro-9*H*-fluoren-2-yl) ethynyl) pyrene (PTN): Compound **3** (200 mg, 0.39 mmol), $PdCl_2(PPh_3)_2$ (27 mg, 0.039 mmol), CuI (3.7 mg, 0.019 mmol), were added to a degassed solution of Et_3N (10 mL) and toluene (20 mL) under nitrogen. Compound **10** (0.730 g, 1.56 mmol) in toluene (5mL) was added slowly. After the mixture was stirred at 70 °C for 12 h, the solvent was removed under reduced pressure and the reaction mixture diluted with ethyl acetate. The resulting solution was filtered through celite. The filtrate was concentrated and the crude product was purified by column chromatography (silica gel, $CHCl_3$-hexane 40/60 v/v) to afford a red colour solid (125 mg, 21% yield). ^{1}H NMR ($CDCl_3$, 300 MHz): δ 0.55-0.77 (m, 40 H), 1.09-1.21 (q, *J* = 7.37 Hz, 16H), 2.07-2.19 (t, *J* = 8.31 Hz, 16H), 7.73-7.92 (m, 16H), 8.23-8.27 (d, *J* = 1.70 Hz, 4H), 8.29-8.35 (d,d, *J* = 8.31, *J* = 1.89 Hz, 4H), 8.61 (s, 2H), 8.92 (s, 4H). ^{13}C NMR ($CDCl_3$, 75 MHz): δ 13.81, 22.97, 25.98, 39.98, 55.85, 89.03, 96.85, 118.33, 119.05, 120.28, 121.39, 123.48, 123.66, 124.25, 126.27, 127.15, 131.34, 131.96, 134.16, 139.37, 146.63, 147.50, 152.27, 152.61. IR (KBr) in cm^{-1}: 737, 824, 1073, 1339, 1460, 1523, 1604, 2860, 2928. MALDI-TOF-MS: (*m*/*z*) $[M^+]$ 1583.7 (100 %) $[M]^+$. Elemental anal. Calc for: C, 81.89: H, 6.49: N, 3.54: O, 8.08. Found: C, 81.84: H, 6.51: N, 3.52: O, 8.11. mp: 296-298 °C, Td: 320 °C.

4. Results and discussion

4. 1. *One-photon absorption and emission spectra.*

The absorption spectra of all the compounds measured in toluene are shown in Fig 1. The relevant peak absorption wavelengths and molar extinction coefficients are presented in Table 1. Two distinct bands are observed in the 1PA spectra - one in the UV-region and the other in the visible region. The band at 260-340 nm in **PMF** and **PDF** and the band at 290-420 nm in **PTF, PTC** and **PTN** arise due to the π→π* transition in the fluorene group. Similarly, the band at 340-480 nm in **PMF** and **PDF** and the band at 420-540 nm in **PTF, PTC** and **PTN** is due to π→π* transition in the pyrene core. The additional band in the spectrum of **PTC** at 200-300 nm is probably due to the absorption of the carbazole fragment. The spectra exhibit a regular bathochromic shift in the λ_{max} from **PMF** to **PTF** in the order of **PMF** (405 nm) < **PDF** (428 nm) < **PTF** (488 nm). The redshift of 23 and 83 nm in the case of **PDF** and **PTF** relative to **PMF** are more likely due to extension of π-conjugation with increase in the number of fluorenylethynyl branches on the pyrene core. The donor (carbazole) and acceptor ($-NO_2$) substituted **PTC** (494 nm) and **PTN** (495 nm) show a very small redshift (6 nm and 7 nm) of the λ_{max} compared to **PTF** (488 nm). On the other hand, in the 290-420 nm region corresponding to the fluorenyl group, **PTC** (385 nm) and **PTN** (391 nm) showed 14 and 20 nm redshift relative to the **PTF** (371 nm), respectively. Based on these trends it is inferred that electron donating or withdrawing groups will have significant

influence on the fluorene moiety and increase the absorption maxima (bathochromic shift).

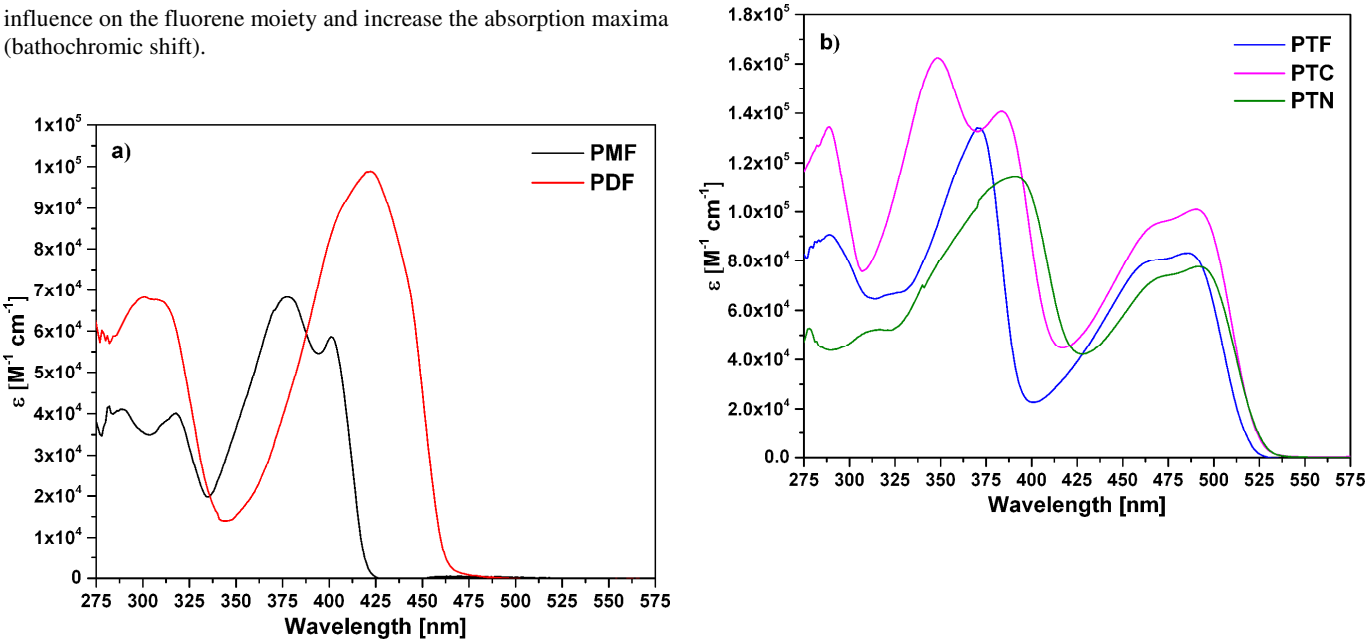

Fig. 1 1PA spectra of a) **PMF** and **PDF** and b) **PTF**, **PTC** and **PTN** compounds measured in toluene at 1 μM concentration.

Table 1 Absorption wavelengths (λ_{max} nm), molar extinction coefficient (ε, M^{-1} cm^{-1}), emission wavelengths (λ_{em}, nm), fluorescence quantum yield (Φ), Stokes shift (cm^{-1}), optical band gap ($E_{0\text{-}0}$, eV) and the ground to first excited state transition dipole moments (μ_{ge}, D) of all the compounds measured in toluene.

Compound	λ_{max} (ε)	$\lambda_{em\ (nm)}$	Φ[a]	Stokes shift	$E_{0\text{-}0}$[b]	μ_{ge}[c]
PMF	405 (58200), 375 (67900), 318 (40100), 288 (41100)	411,436	0.95	360	405(3.06)	6.1
PDF	428 (98900), 303 (67900)	453,480	0.98	1290	445(2.79)	16.2
PTF	488 (80900), 462 (79100), 371 (134000), 289 (90300)	513,548	0.59	1000	501(2.48)	8.7
PTC	494 (99700), 467 (94600), 385 (140000), 348 (162000)	518,554	0.56	940	505(2.46)	15.0
PTN	495 (77100), 468 (72600), 391 (114000), 311 (52000)	520,556	0.55	970	508(2.44)	8.7

[a] Fluorescence quantum yield measured relative to diphenylanthracene (Φ = 0.9 ± 0.1 in cyclohexane) as standard.
[b] $S_0 \rightarrow S_1$ energy gap ($E_{0\text{-}0}$)_is obtained from the intercept of absorption and emission spectra.
[c] The experimental $S_0 \rightarrow S_1$ transition dipole moments are obtained by computing the area under each peak using the equation where, $\mu_{ge}^2 = \frac{1500\ln(10)\hbar cn}{2\pi^2 N_A}\int\frac{\varepsilon(\bar{\nu})}{\bar{\nu}}d\bar{\nu} = 9.18358\times10^{-39}\times n\int\frac{\varepsilon(\bar{\nu})}{\bar{\nu}}d\bar{\nu}$; where n is refractive index of the solvent (in our case, n = 1.496 for toluene), c is velocity of light, 3×10^{10} cm/sec, N_A is Avogadro number, ε is molar extinction coefficient (obtained from absorption spectra), ν is wavenumber in cm^{-1} and $\hbar = \frac{h}{2\pi} = 1.054\times10^{-27}$ erg.sec . The integral $\int\frac{\varepsilon(\bar{\nu})}{\bar{\nu}}d\bar{\nu}$ refers to the area under the curve of a plot with $\frac{\varepsilon(\bar{\nu})}{\bar{\nu}}$ as the abscissa and $\bar{\nu}$ as the ordinate of the absorption spectra.

The nature of the transitions at the molecular level can be easily understood based on the quantum chemical calculations. The calculated 1PA wavelengths, ground- and excited-state dipole moments, transition dipole moments, and the nature of transitions in the gas phase are given in Table 2. The corresponding maximum wavelengths for **PMF**, **PDF**, **PTF**, **PTC** and **PTN** are 370, 414, 478, 482 and 484 nm ($1^1A' \rightarrow 2^1A'$ (**PMF**)/$1^1A \rightarrow 1^1B$ (**PTC**)/$1^1A_u \rightarrow 1^1B_u$ (**PDF**, **PTF, PTN**); π→π*) respectively. These wavelengths are in good agreement with the experimental values and trends for redshift: **PMF** < **PDF** < **PTF** < **PTC** ≈ **PTN**. The redshift in these molecules is attributed to the increased π-electron delocalization with the increase of conjugation length, as well as some fractional charge transfer, which indicating appreciable electronic coupling between the orbitals of the pyrene core and ethynylfluorenyl fragments favouring the small HOMO-LUMO gap. This fact is evident from the localization of electron densities in the fragment orbitals at the positions connecting these fragments as shown in Fig. 2, (top) indicating that **PTF** and **PTC** can be considered, as D–π–A–π–D structures and **PTN** as an A–π–D–π–A type of structural motif, respectively. The respective $S_0 \rightarrow S_1$ transition dipole moments, μ_{ge} are also large, ranging between 10.7 to 14.8 D and follow the order **PMF** < **PTF** < **PTN** < **PTC** < **PDF** for both measured and calculated values. PDF has larger μ_{ge} of 14.8 D (measured 16.2 D)

compared to the tetra-branched chromophores **PTF** (13.6 D), **PTC** (14.7 D) and **PTN** (14.3 D). This is likely due to the fact that the **PDF** does not retain its symmetry in the excited state, i.e it undergoes symmetry breaking and the geometry attains dipolar structure (non-zero dipole moment or zwitterionic in nature) in the excited state, which is stabilized relative to the ground state. However, relaxation of the geometry in the excited state reduces the dipolar character and subsequently the ratio of mixing between the neutral and zwitterionic states changes. This leads to increase of the overlap between the HOMO and LUMO wavefunctions and a larger emitting transition dipole moment (14.8 D). While for **PTF, PTC** and **PTN** have combined dipolar and quadrupolar characteristics. The interaction between the dipolar branches in the excited state shows up in the quadrupolar character. For, symmetry reasons, these tetra-branched chromophores upon excitation, undergo a two-dimensional intramolecular charge transfer from branches to pyrene core (**PTF** and **PTC**) or from pyrene core to the branches (**PTN**). In addition, even though the overall molecular dipole moments of the ground and excited states are similar compared to the single-branched molecule **PMF** due to symmetry reasons their local dipole moments on the emitting branches are also very similar. Further, the interaction between the dipolar branches lifts the degeneracy between the excited states, generating a number of charge transfer states which are 1PA allowed and thus leads to large shift in the absorption wavelength by ~110 nm (~86 nm experimental shift) compared to **PMF** and the net decrease in μ_{ge} compared to **PDF**. This indicates that the conjugation is helpful for enhancing 1PA and branch-branch interactions is helpful for increasing the number of charge transfer states. Furthermore, at the orbital level, these transitions are described as a single particle-hole excitations from the HOMO to LUMO level as evident form the large CI coefficients (>~90%, Table 2) and from the one-electron frontier molecular orbitals as shown in the Fig. 2 (bottom).

Table 2 Calculated 1PA wavelength (λ_{1PA}, nm), symmetry of the states, ground-, excited-state dipole moments (μ_g, μ_e, D), $S_0 \rightarrow S_1$ transition dipole moments (μ_{ge}, D) and their nature.

Molecule	λ_{1PA}	State	μ_g	μ_e	μ_{ge}	Nature
PMF	370	$1^1A' \rightarrow 2^1A'$	0.5	1.1	10.7	(92.2%) HOMO→LUMO
PDF	414	$1^1A_g \rightarrow 1^1B_u$	0.0	0.0	14.8	(91.2%) HOMO→LUMO
PTF	478	$1^1A_g \rightarrow 1^1B_u$	0.0	0.0	13.6	(92.8%) HOMO→LUMO
PTC	482	$1^1A \rightarrow 1^1B$	0.1	0.1	14.7	(91.5%) HOMO→LUMO
PTN	484	$1^1A_g \rightarrow 1^1B_u$	0.0	0.0	14.3	(89.2%) HOMO→LUMO

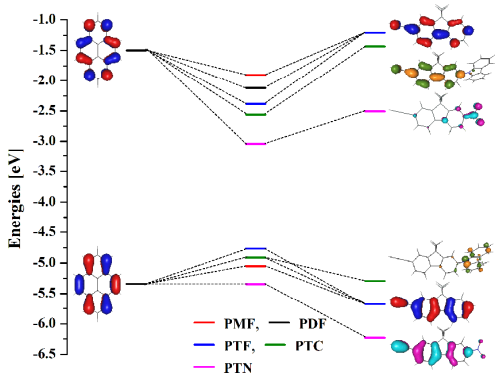

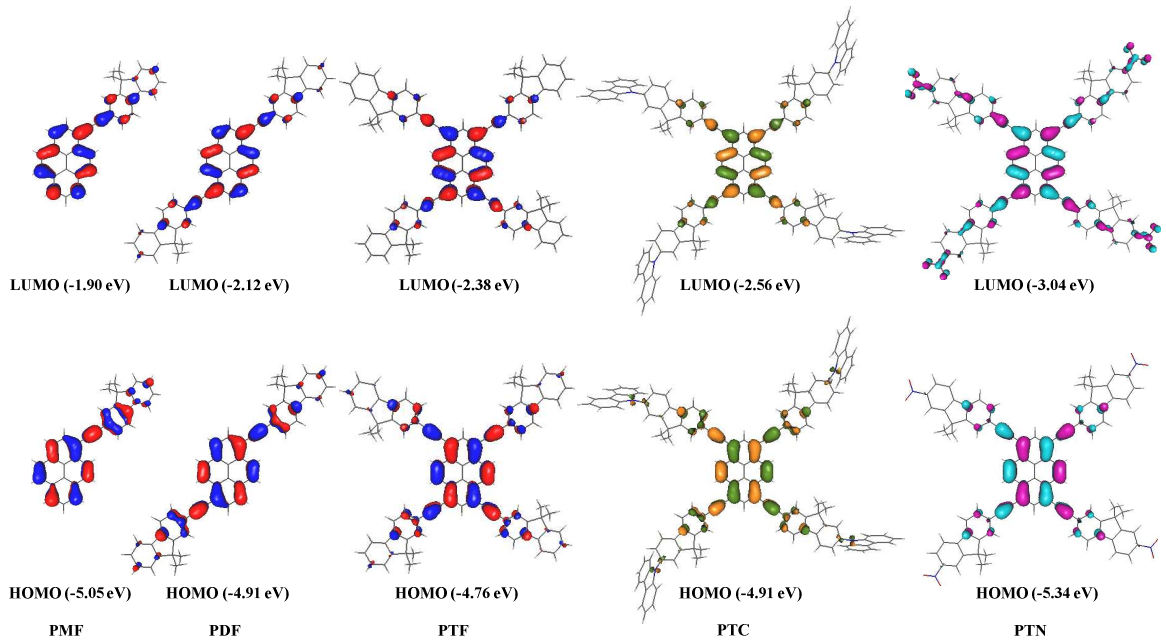

Fig. 2 The pyrene core fragment and ethynylfluorenyl fragment orbitals (top) and the one-electron frontier molecular orbitals (bottom) obtained at B3LYP/6-31G** level of the theory.

For evaluating the solvatochromism, the UV-visible spectra of all the compounds were measured in solvents with varied polarities: hexane, toluene, tetrahedrofuran, chloroform, methanol and acetonitrile (Fig. S1 and Table S1 in supporting information). The spectra of **PTF** in methanol and acetonitrile and that of **PTN** in hexane were not obtained due to lack of solubility. Generally, solvatochromism depends on the extent of charge separation in the excited state of a chromophore. The influence of solvent polarity on absorption wavelengths is very small or negligible in case of **PMF, PDF** and **PTF**, indicating negligible intramolecular charge-transfer in the ground state. **PTC** showed a slight positive solvatochromism of 762 cm^{-1} on going from hexane to acetonitrile while **PTN** showed a considerable positive solvatochromism of 1226 cm^{-1} from toluene to acetonitrile indicates the presence of small amount of charge transfer in the ground state. We have carried out concentration dependent UV-Vis absorption studies (Fig S2, supporting information) to rule out the possibility of aggregation contributing the red shifted absorption in MeOH and Acetoniotrile solvenrts for PTC and PTN. Based on this, it is suggested that the origin of these solvatochromic shifts in acetonitrile and methanol for **PTC** and **PTN** may be due to the solute quadrupole-solvent dipole interaction[79]. The carbazole with N-C bond attached to fluorene in **PTC** and strong polarizing NO_2 group attached to fluorene in **PTN** exerts efficient interaction with highly polar solvents like methanol and acetonitrile. These interactions will stabilize the excited state more than the ground state, resulting in a decrease in energy for electronic transitions and a bathochromic shift is observed in solvents with higher dipole moment.

To describe quantitatively this solvent dependence, we studied the correlation of the band position (transition energy) versus the solvent polarity using the Lippert's polarity function, defined as $F(n,\varepsilon)=\frac{1-n^2}{1+2n^2}-\frac{1-\varepsilon}{1+2\varepsilon}$, where n and ε are the solvent refractive index and dielectric constant, respectively.[27, 80] For all the studied dyes, almost linear dependence on the solvent polarity is observed (Fig. S3a). The resulting slopes are listed in Table S2. Interestingly, while **PMF** shows relatively large positive slope of 1009 cm^{-1}, other compounds show negative slopes of the comparable magnitudes. This shows that the **PMF** it has a sizable permanent dipole moment in the ground state due to its non-centrosymmetric nature. On the other hand, the solvatochromic shifts of other compounds are affected by quadrupolar interactions and also by the change of the molecular geometry in the excited state.

The fluorescence spectra of all the compounds are measured in toluene and are shown in Fig. 3. The spectra showed two vibronically resolved peaks and a bathochromic shift is observed in the order of **PMF** (436 nm) **< PDF** (480 nm) **< PTF** (548 nm) **< PTC** (554 nm) **< PTN** (556 nm) independent of the excitation wavelength. The peak wavelengths are summarized in Table 1. These observations indicate that the energy gap between the ground- and excited-states decrease in the order of **PMF > PDF > PTF > PTC > PTN**. Furthermore, all these compounds showed large Stokes shifts ranging from 360 to 1290 cm^{-1} (Table 1) and relatively large fluorescence quantum yields (Φ) ranging from 0.95 and 0.98 for **PMF** and **PDF** to ~0.5 for **PTF**, **PTC** and **PTN**.

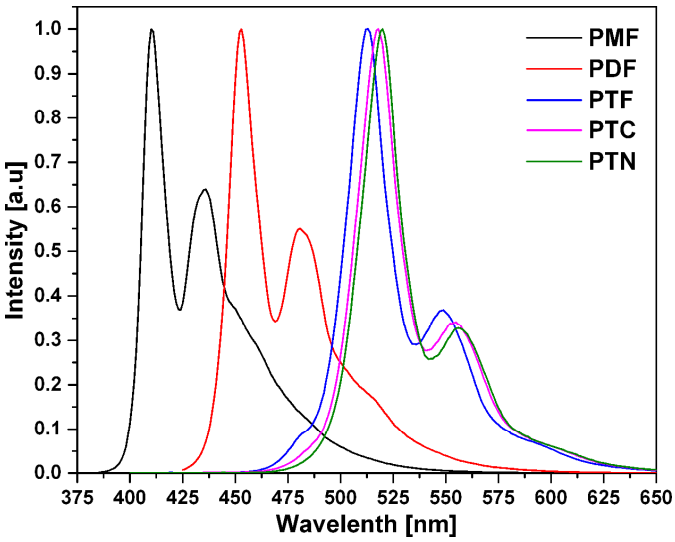

Fig. 3 Normalized fluorescence spectra of all the compounds measured in toluene at 1μ M concentration, excited at their corresponding λ_{max}.

The solvatochromic effects of the fluorescence spectra were also measured in solvents with varying polarity (same solvents as used for the UV-Vis spectra) (Fig. S4 and Table S1, Supporting Information). Compounds **PMF**, **PDF** and **PTF** show small fluorescence solvatochromism, with two resolved vibronically coupled peaks, indicating the presence of small intramolecular charge transfer in the excited state. In the case of the **PTC** and **PTN**, the emission spectra of the two fluorophores are more sensitive to the solvent (Fig. S4): in both cases, as the solvent polarity increases, the spectra are red-shifted, and are much less intense. For example, going from nonpolar hexane to polar methanol, the emission of **PTC** redshifts by 2820 cm^{-1}, and going from nonpolar toluene to polar methanol, the emission of **PTN** redshifts by 2730 cm^{-1}. It suggested that the excited states of these compounds **PTC** and **PTN** posses more polar character, and more polar environments efficiently enhanced the intramolecular charge transfer from carbazole to pyrene acceptor[81] in **PTC** and pyrene to Nitro group in case of **PTN**. The solvent dependence of emission spectra indicates strong ICT in the excited state. The stronger the solute/solvent interaction, the lower the energy of the excited state, and the larger the red shift of the emission band and the corresponding Stokes shift. The solvatochromic behaviour is accompanied by a decrease of the fluorescence quantum yield when the polarity of the solvent increases (Table **S1** in supporting information) is also an indication that the excited state possess is ICT.[82]

To describe quantitatively this solvent dependence, we studied the correlation of the band position (transition energy) versus the solvent polarity index. For all the studied dyes, an almost linear dependence on the solvent polarity is observed (Fig. S3b). The resulting slopes are listed in Table S2.

4. 2. *Two-Photon and Excited-State Absorption Spectra*

In order to characterize the suitability of the compounds for 2PA applications, the measurements of their 2PA spectra and cross-sections were performed in toluene and recorded by using two-photon excited fluorescence method (Fig. 4). The obtained parameters are tabulated in Table 3. Fig. 4 shows 1PA and 2PA spectra of the compounds plotted versus the transition wavelengths to facilitate easier comparison.

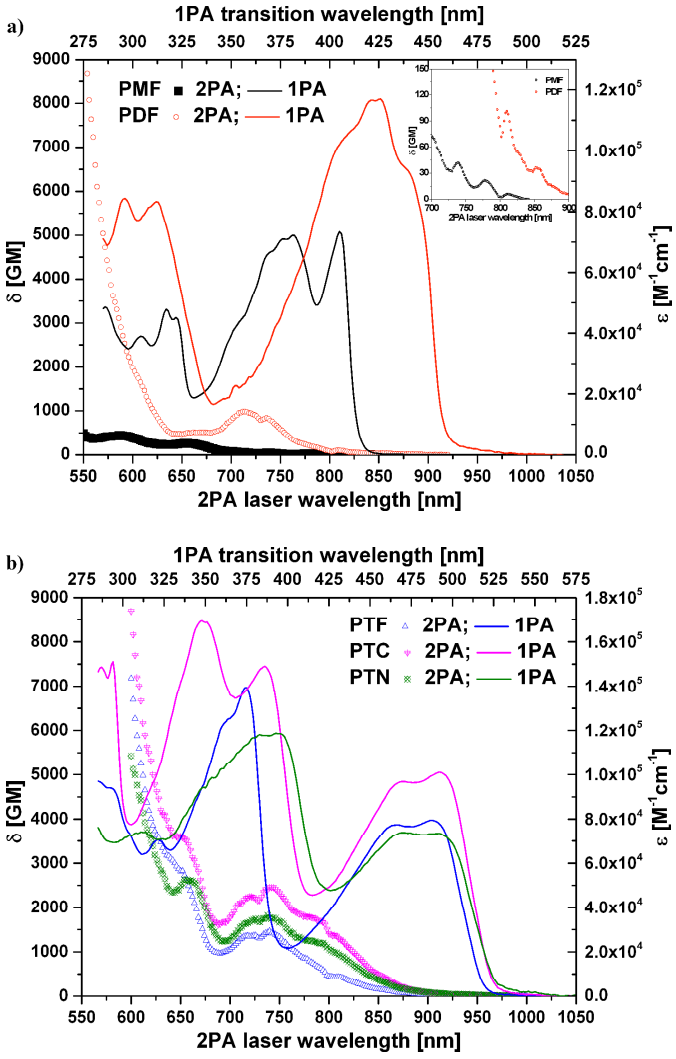

Fig. 4 2PA spectra of a) **PMF** and **PDF** and b) **PTF**, **PTC** and **PTN** measured in toluene. For comparison, 1PA spectra are shown in the same figure.

Fig. 4a shows 2PA spectra of the compounds **PMF** and **PDF**. The single-branch compound **PMF** exhibits relatively weak 2PA, with δ below 500 GM. The spectrum consists of five peaks at ~810 nm (6 GM), 780 nm (22 GM), 740 nm (42 GM), ~655 nm (260 GM), and ~585 nm (450 GM), a shoulder at ~705 nm (66 GM), and also demonstrates a slight increase towards short wavelengths, ~550 nm (480 GM) (weak long-wavelengths peaks are shown in inset of Fig. 4a). The longest wavelength peak corresponds in its position to the lowest energy transition in the 1PA. The third 2PA peak and a shoulder also correspond to the peak and shoulder in the 1PA spectrum, respectively. Other peaks do not correspond to the 1PA peaks, and instead appear at the positions of minima in the 1PA spectrum. The peaks at 810 nm and 740 nm reveal the non-symmetrical character of the molecule (as the selection rules in centrosymmetrical molecules require states of the opposite parity to be allowed in 1PA and 2PA, while the selection rules are relaxed in non-symmetrical molecules, and thus the same transitions can appear in the 1PA and 2PA spectra), while the other peaks show strong coupling between the pyrene and fluorene constituencies. Contrary to the **PMF** molecule, the **PDF** spectrum shows a weak shoulder in the range of the lowest energy transition (~840 nm, 42 GM), and a

much stronger peak at ~715 nm (990 GM). The sharp increase towards short wavelengths reaches almost 9000 GM, as the 2PA cross-sections are significantly enhanced when the denominator of the 2PA transition matrix (see equation 1) approaches zero as the laser frequency v approaches the one-photon $S_0 \rightarrow S_1$ transition maximum v_{10}. This effect is commonly referred to as a pre-resonance enhancement when the excitation wavelength approaches 1PA transition.[83-85]

Fig. 4b shows 2PA spectra of the tetra-branched compounds **PTF, PTC** and **PTN**. All three compounds show a weak shoulder in the range of the lowest energy transition (~950 nm, <25 GM), a strong peak at ~740 nm, reaching 1500-2500 GM, a shoulder at ~650 nm, and a sharp increase towards shorter wavelengths. At the wavelengths longer than 650 nm, the 2PA strength increases on going from **PTF** to **PTN** to **PTC**, while at shorter wavelengths the δ for **PTN** is lower than that of the **PTF**. Based on these results we can conclude that as the number of branches increases the peak cross-sections increases. Substituents with stronger electron donating or withdrawing character enhance the peak cross-sections while the neutral substituents lead to smaller cross-sections. Interestingly molecules **PTC** and **PTN** show higher 2PA cross-sections than most of the other small molecules reported[47, 86-88] with similar 2PA wavelengths. The strong 2PA cross-sections and good quantum yields make these dyes good candidates with high two-photon brightness, for example a brightness of ~1400 GM for PTC (Table 3).

Table 3 Experimental 2PA wavelength (λ_{2PA}, nm), peak 2PA cross-sections (δ, GM), first excited state to the 2PA state transition dipole moments ($\mu_{ee'}$, D) and 2PA brightness ($\delta \times \Phi_{fl}$, GM).

Compound	λ_{2PA}	δ	$\delta \times \Phi_{fl}$	$\mu_{ee'}$
PMF	650	260	247	6.3
PDF	710	990	970	8.9
PTF	740	1460	861	10.8
PTC	740	2460	1377	12.1
PTN	740	1820	1001	11.1

The ESA spectra of the compounds are shown in Fig. 5. At short probe wavelengths, ~400-500 nm, the spectra display ground state bleach corresponding to their 1PA bands. At probe wavelengths >500 nm all the spectra show several broad ESA bands, comparable in strength to their lowest-energy 1PA. Using **PMF** as an example compound (see energy schematic, Fig. 5b), we can discuss observed ESA bands in relation to the 1PA and 2PA spectra. While the non-centrosymmetric nature of the compound is responsible for 2PA at S_1 peak, 3-level pathways are operative for the higher-energy transitions. For the S_i 2PA peak to be strong, one of the dominant pathways would require allowed transitions $S_0 \rightarrow S_1$ and $S_1 \rightarrow S_i$. Thus, slight increase in ESA towards 1600 nm probe wavelength, which probably peaks at ~1700 nm not accessible in our setup, indicates that the $S_0 \rightarrow S_8$ transition is 2PA allowed (arise as $S_0 \rightarrow S_1$ 1PA and $S_1 \rightarrow S_8$ ESA, shown on schematic by red arrow). This indeed is observed experimentally, while the 1PA spectrum exhibit minimum at the corresponding transition energy. Similarly, ESA peak at ~1170 nm and a shoulder at ~1030 nm both contribute to the 2PA-allowed transition $S_0 \rightarrow S_{12}$, which appears near 1PA minimum. The strength of the ESA bands correlates with the enhanced 2PA for the same transitions as compared to the lower-energy bands. Similarly, **PDF** ESA bands at ~830 nm, 980 nm, 1170 nm, and >1600 nm also correspond to the transitions to 2PA active states.

Tetra-branched compounds also show broad and strong ESA corresponding to their transitions from the first excited state to the fluorene-centered excited states (290-420 nm absorption bands). The ESA band appearing at >1600 nm is probably responsible for the strong 2PA transition seen at ~740 nm for these compounds (see transitions $S_1 \rightarrow S_5$ and $S_1 \rightarrow S_6$ for **PTF**, schematic Fig. 5d), while the ESA shoulder at ~1370 nm corresponds to the 2PA peak around 715 nm ($S_1 \rightarrow S_7$ and $S_1 \rightarrow S_8$). The pronounced ESA peak at ~980 nm corresponds to a $S_1 \rightarrow S_{13}$ transition (for **PTF**), which is realized in our experimental 2PA spectrum as a sharp increase towards short wavelengths.

From the peak absorptivities of the ESA spectra at ~600-1600 nm, the transition dipole moments between the lowest one-photon state and the two-photon state, $\mu_{ee'}$ were calculated and are shown in Table 3. The trend observed for $\mu_{ee'}$ follows the order of the 2PA cross-sections at ~600-650 nm for **PMF** and **PDF** and ~740 nm for **PTF**, **PTN**, and **PTC**, suggesting that the 3-level pathway is the dominant contribution to the δ of these compounds.

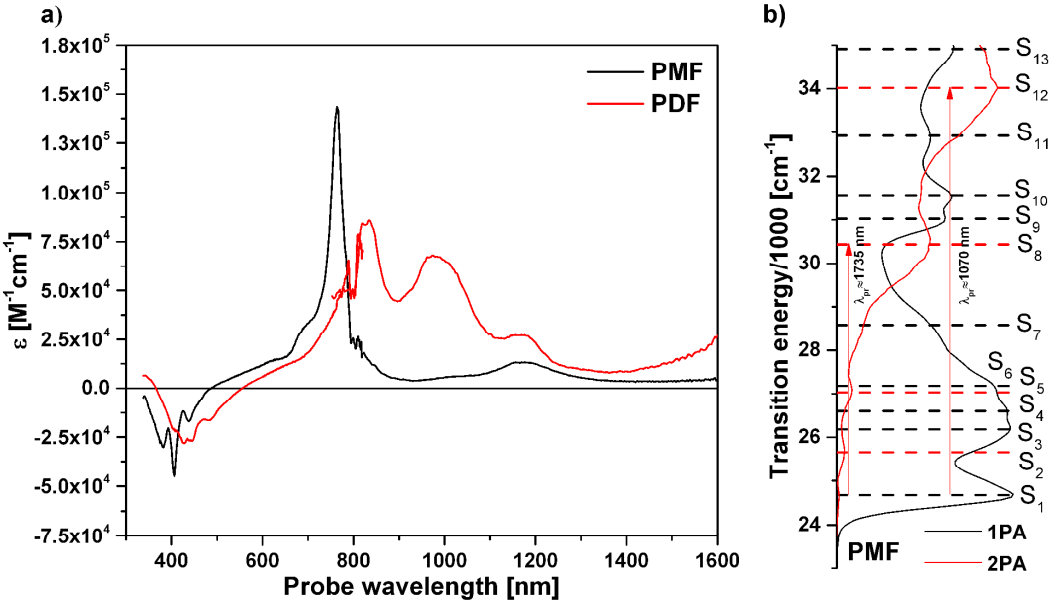

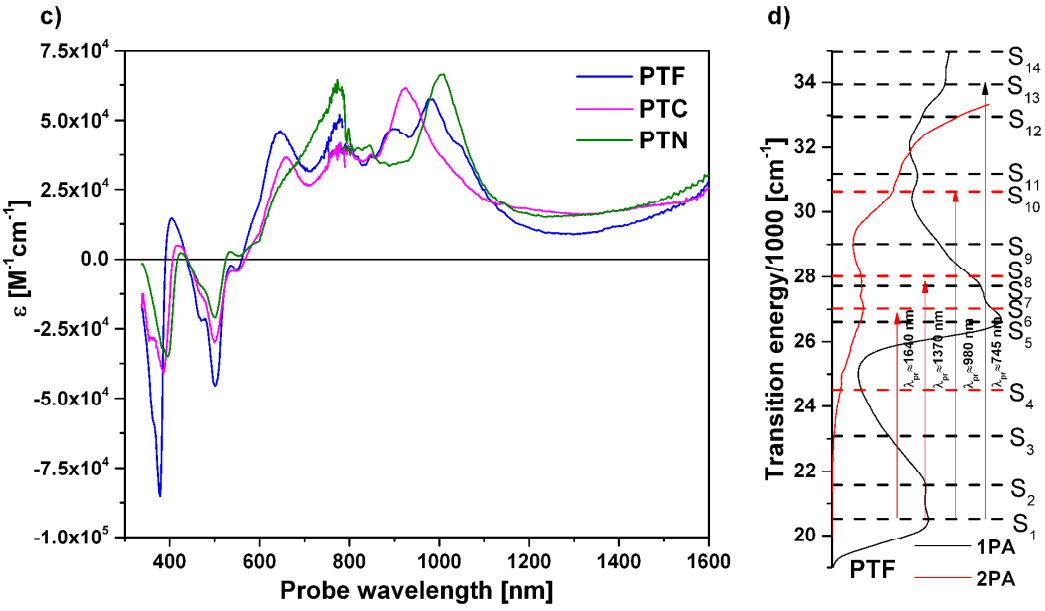

Fig. 5 Excited-state absorption spectra of a) **PMF** and **PDF** and c) **PTF**, **PTC** and **PTN** measured in toluene. Also shown are approximate level diagrams for b) **PMF** and d) **PTF**.

4.3. Theoretical Study on Two-Photon Absorption Spectra

The calculated δ for the lowest five excited states are presented in Table 4. It is observed that irrespective of number of branches, one can notice that the lowest energy band (corresponding to the most intense OPA.)[1] is two-photon forbidden (very small or negligible cross-section were obtained, Table 4) as can be predicted by symmetry. From the Table 4 it is clear that among all the compounds, **PMF** has the weakest δ of 180 GM located at 536 nm. Referring to **PDF** with increased π-electron delocalization, the δ increased by ~5 times, 860 GM at 592 nm. It also has a strong peak of 721 GM at 515 nm. In the case of tetra-branched molecules **PTF**, **PTN**, and **PTC**, it is interesting to see that the next four higher excited states are 2PA active due to strong coupling between the dipolar branches (as evident from the broadening of the spectra in the region 700-850 nm). **PTC** showed larger δ among the three with magnitude of 1300 GM at 623 nm followed by **PTN** and **PTF** with magnitudes of 1040 GM at 642 nm and 801 GM at 612 nm. The four 2PA states appeared due to four coupling combinations among the branches (branch1-branch2, branch1-branch3, branch2-branch3 and branch3-branch4). This coupling interaction is responsible for the splitting between the degenerate excited states. The splitting between these 2PA states amounts to ~0.05-0.30, ~0.07-0.25 and ~0.05-0.30 eV i.e. ~400-2400 cm^{-1} (includes all four interactions among the branches) respectively for **PTF**, **PTN**, and **PTC**. Thus, these interactions lead to a cooperative enhancement of 2PA cross-sections. Furthermore, one can see that the theoretical values are generally consistent with the measured values in trends. The calculated values are, however, are smaller than the measured ones. This discrepancy is probably due to the fact that the theoretical stimulations give the intrinsic δ contributed by the electronic motion in gas phase. The vibronic coupling contribution is not considered here. Furthermore, the experimental measurements are performed in solutions; thus, the interactions between the solvent and solute molecules may have influence on the optical properties of these compounds. Therefore, from the calculations, one may conclude that the tetra-substitution enhances the 2PA cross-sections in these compounds and at the same time, the symmetry of the structures has a great influence on the δ. These observations lead to the following structure-property relationships via modifications on the pyrene core for enhanced 2PA cross-sections: (i) increasing the length of conjugation, (ii) appropriate tuning of the number of branches and the coupling between them, (iii) increasing the number of charge transfer states through branch-branch interactions facilitated by tetra-substitution, (iv) symmetry of the structures, i.e. higher the symmetry, larger the cross-section and (v) intramolecular charge transfer from the core to the periphery or periphery to the core could constitute a substantial way for obtaining amplification of the aimed properties in the desired spectral regions, and (vi) substituents with stronger electron donating or withdrawing character enhance the peak cross sections while the neutral substituents lead to smaller cross sections.

Table 4 Calculated transition wavelength (λ_{2PA}, nm) and peak 2PA cross-sections (δ, GM) for the lowest five excited states.

State	PMF		PDF		PTF		PTC		PTN	
	λ_{2PA}	δ	λ_{2PA}	δ	λ_{2PA}	δ	λ_{2PA}	δ	λ_{2PA}	δ

1	740	0.08	648	22	695	23.5	715	35.8	725	28
2	646	3	592	860	646	466	661	536	667	501
3	581	0.6	533	2.5	631	371	636	620	648	485
4	536	180	524	4.6	612	801	623	1300	642	1040
5	524	1.4	515	721	559	310	584	130	573	410

5. Conclusion

A new series of D–π–A, D–π–A–π–D and A–π–D–π–A based fluorenylethynylpyrene derivatives: with mono- **(PMF)**, di- (**PDF**) and tetra-branched (**PTF, PTC**, and **PTN**) fluorenyl groups on periphery linked to pyrene by acetylene π-bridge have been synthesized in good yields and characterized by all spectral methods. According to experimental measurements large Stokes shifts with significant fluorescence quantum yields and high photostability were achieved for these compounds. The 2PA cross-sections of all the compounds show high values ranging from ~250 to ~2500 GM in the order of **PMF < PDF < PTF < PTN < PTC**, in the wavelength range suitable for biological/biomedical applications (650-900 nm). Substituents with stronger electron donating or withdrawing character enhance the peak cross-sections while the unbiased substituent lead to smaller cross-sections. The highest 2PA value in **PTC** (2460 GM) is achieved due to a large charge transfer between the excited states from the carbazole unit to the fluorenyl unit and to the pyrene acceptor. 2PA of **PTN** is 1820 GM, smaller than that for **PTC**, most probably, due to the interaction of $–NO_2$ group with the solvent rather than the electronic coupling between the molecular fragments. Interestingly these small molecules **PTC** and **PTN** with large quantum yields and short absorption wavelengths show higher 2PA cross-sections than the other small molecules reported with similar 2PA wavelengths. Thus the strategy of enhancing the electronic communication by increasing planarity between donor and acceptor moiety and increasing electron donating power of donor proved ideal for obtaining large two-photon absorption cross-sections. Combining large 2PA cross sections with large fluorescence quantum yields make these chromophores promising probes with large 2PA brightness.

References

1. M. Pawlicki, H. A. Collins, R. G. Denning and H. L. Anderson, *Angew. Chem., Int. Ed.*, 2009, 48, 3244-3266.
2. F. Terenziani, C. Katan, E. Badaeva, S. Tretiak and M. Blanchard-Desce, *Adv. Mater.*, 2008, 20, 4641-4678.
3. T.-C. Lin, Y.-Y. Liu, M.-H. Li, C.-Y. Liu, S.-Y. Tseng, Y.-T. Wang, Y.-H. Tseng, H.-H. Chu and C.-W. Luo, *Chem. Asian J.*, 2014, 9, 1601-1610.
4. T.-H. Huang, Y.-H. Wang, Z.-H. Kang, J.-B. Yao, R. Lu and H.-Z. Zhang, *Photochem. Photobiol.*, 2014, 90, 29-34.
5. M. G. Vivas, D. L. Silva, L. De Boni, Y. Bretonniere, C. Andraud, F. Laibe-Darbour, J. C. Mulatier, R. Zaleśny, W. Bartkowiak, S. Canuto and C. R. Mendonca, *J. Phys. Chem. B*, 2012, 116, 14677-14688.
6. R. D. Breukers, S. Janssens, S. G. Raymond, M. D. H. Bhuiyan and A. J. Kay, *Dyes Pigm.*, 2015, 112, 17-23.
7. G. S. He, L.-S. Tan, Q. Zheng and P. N. Prasad, *Chem. Rev.*, 2008, 108, 1245-1330.
8. M. Pawlicki, H. A. Collins, R. G. Denning and H. L. Anderson, *Angew. Chem., Int. Ed.*, 2009, 48, 3244-3266.
9. H. Myung Kim and B. Rae Cho, *Chem. Commun.*, 2009, 153-164.
10. A. S. Dvornikov, E. P. Walker and P. M. Rentzepis, *J. Phys. Chem. A*, 2009, 113, 13633-13644.
11. B. H. Cumpston, S. P. Ananthavel, S. Barlow, D. L. Dyer, J. E. Ehrlich, L. L. Erskine, A. A. Heikal, S. M. Kuebler, I. Y. S. Lee, D. McCord-Maughon, J. Qin, H. Rockel, M. Rumi, X.-L. Wu, S. R. Marder and J. W. Perry, *Nature*, 1999, 398, 51-54.
12. H. Tian and Y. Feng, *J. Mater. Chem.*, 2008, 18, 1617-1622.
13. C. Barsu, R. Cheaib, S. Chambert, Y. Queneau, O. Maury, D. Cottet, H. Wege, J. Douady, Y. Bretonniere and C. Andraud, *Org. Biomol. Chem.*, 2010, 8, 142-150.
14. C. N. LaFratta, J. T. Fourkas, T. Baldacchini and R. A. Farrer, *Angew. Chem., Int. Ed.*, 2007, 46, 6238-6258.
15. T.-C. Lin, Y.-J. Huang, Y.-F. Chen and C.-L. Hu, *Tetrahedron*, 2010, 66, 1375-1382.
16. W. S. Charles, *J. Mater. Chem.*, 1999, 9, 2013-2020.
17. K. Ogawa, H. Hasegawa, Y. Inaba, Y. Kobuke, H. Inouye, Y. Kanemitsu, E. Kohno, T. Hirano, S.-I. Ogura and I. Okura, *J. Med. Chem.*, 2006, 49, 2276-2283.
18. S. Kim, T. Y. Ohulchanskyy, H. E. Pudavar, R. K. Pandey and P. N. Prasad, *J. Am. Chem. Soc.*, 2007, 129, 2669-2675.

Acknowledgements

The authors thank Director of Indian Institute of Chemical Technology, for the encouragement. Authors at IICT acknowledge CSIR 12th plan INTEL COAT project CSC-0201 for financial assistance. C.L.D and K.Y thank the council of Scientific and Industrial Research, New Delhi for Research Fellowship. The work at Georgia Tech was supported in part by the DARPA ZOE Program (Grant No. W31P4Q-09-1-0012) and the Army Research Office, Defence University Research Instrumentation Program (Grant No. 59287CHRIP).

Notes and references

[a] *Crop Protection Chemicals Division,* [b] *Inorganic and Physical Chemistry Division,* [e]*AcSIR, CSIR-Indian Institute of Chemical Technology, Uppal Road, Tarnaka, Hyderabad - 500 007, India.*

[c] *School of Chemistry and Biochemistry and Center for Organic Photonics and Electronics, Georgia Institute of Technology, Atlanta, Georgia 30332-0400, United States.*

[d] *Currently at Center for Advanced Solar Photophysics, Los Alamos National Laboratory, Los Alamos, New Mexico 87545, United States.*

Corresponding Authors: jrao@iict.res.in

Electronic Supplementary Information (ESI) available. See DOI: 10.1039/x0xx00

19. G. J. Brakenhoff, M. Muller and R. I. Ghauharali, *J. Microsc.*, 1996, 183, 140-144.
20. O. A. Vydrov and G. E. Scuseria, *J. Chem. Phys.*, 2006, 125, 234109-234109.
21. O. A. Vydrov, J. Heyd, A. V. Krukau and G. E. Scuseria, *J. Chem. Phys.*, 2006, 125, 074106-074109.
22. S. Zheng, A. Leclercq, J. Fu, L. Beverina, L. A. Padilha, E. Zojer, K. Schmidt, S. Barlow, J. Luo, S.-H. Jiang, A. K. Y. Jen, Y. Yi, Z. Shuai, E. W. Van Stryland, D. J. Hagan, J.-L. Brédas and S. R. Marder, *Chem. Mater.*, 2007, 19, 432-442.
23. A. Bhaskar, G. Ramakrishna, Z. Lu, R. Twieg, J. M. Hales, D. J. Hagan, E. Van Stryland and T. Goodson, *J. Am. Chem. Soc.*, 2006, 128, 11840-11849.
24. P. Wei, X. Bi, Z. Wu and Z. Xu, *Org. Lett.*, 2005, 7, 3199-3202.
25. C.-F. Chou, T.-H. Huang, J. T. Lin, C.-C. Hsieh, C.-H. Lai, P.-T. Chou and C. Tsai, *Tetrahedron*, 2006, 62, 8467-8473.
26. C. Lavanya Devi, K. Yesudas, N. S. Makarov, V. Jayathirtha Rao, K. Bhanuprakash and J. W. Perry, *Dyes Pigm.*, 2015, 113, 682-691.
27. N. S. Makarov, S. Mukhopadhyay, K. Yesudas, J.-L. Brédas, J. W. Perry, A. Pron, M. Kivala and K. Müllen, *J. Phys. Chem. A*, 2012, 116, 3781-3793.
28. B. A. Reinhardt, L. L. Brott, S. J. Clarson, A. G. Dillard, J. C. Bhatt, R. Kannan, L. Yuan, G. S. He and P. N. Prasad, *Chem. Mater.*, 1998, 10, 1863-1874.
29. W. J. Yang, D. Y. Kim, M.-Y. Jeong, H. M. Kim, Y. K. Lee, X. Fang, S.-J. Jeon and B. R. Cho, *Chem. Eur. J.*, 2005, 11, 4191-4198.
30. W. J. Yang, C. H. Kim, M.-Y. Jeong, S. K. Lee, M. J. Piao, S.-J. Jeon and B. R. Cho, *Chem. Mater.*, 2004, 16, 2783-2789.
31. R. Kannan, G. S. He, L. Yuan, F. Xu, P. N. Prasad, A. G. Dombroskie, B. A. Reinhardt, J. W. Baur, R. A. Vaia and L.-S. Tan, *Chem. Mater.*, 2001, 13, 1896-1904.
32. D.-X. Cao, Q. Fang, D. Wang, Z.-Q. Liu, G. Xue, G.-B. Xu and W.-T. Yu, *Eur. J. Org. Chem.*, 2003, 2003, 3628-3636.
33. M. Rumi, J. E. Ehrlich, A. A. Heikal, J. W. Perry, S. Barlow, Z. Hu, D. McCord-Maughon, T. C. Parker, H. Röckel, S. Thayumanavan, S. R. Marder, D. Beljonne and J.-L. Brédas, *J. Am. Chem. Soc.*, 2000, 122, 9500-9510.
34. O.-K. Kim, K.-S. Lee, H. Y. Woo, K.-S. Kim, G. S. He, J. Swiatkiewicz and P. N. Prasad, *Chem. Mater.*, 2000, 12, 284-286.
35. L. Ventelon, S. Charier, L. Moreaux, J. Mertz and M. Blanchard-Desce, *Angew. Chem., Int. Ed.*, 2001, 40, 2098-2101.
36. O. Mongin, L. Porrès, L. Moreaux, J. Mertz and M. Blanchard-Desce, *Org. Lett.*, 2002, 4, 719-722.
37. Z.-Q. Liu, Q. Fang, D.-X. Cao, D. Wang and G.-B. Xu, *Org. Lett.*, 2004, 6, 2933-2936.
38. S.-J. Chung, S. Zheng, T. Odani, L. Beverina, J. Fu, L. A. Padilha, A. Biesso, J. M. Hales, X. Zhan, K. Schmidt, A. Ye, E. Zojer, S. Barlow, D. J. Hagan, E. W. Van Stryland, Y. Yi, Z. Shuai, G. A. Pagani, J.-L. Brédas, J. W. Perry and S. R. Marder, *J. Am. Chem. Soc.*, 2006, 128, 14444-14445.
39. S. K. Lee, W. J. Yang, J. J. Choi, C. H. Kim, S.-J. Jeon and B. R. Cho, *Org. Lett.*, 2004, 7, 323-326.
40. S.-I. Kato, T. Matsumoto, T. Ishi-I, T. Thiemann, M. Shigeiwa, H. Gorohmaru, S. Maeda, Y. Yamashita and S. Mataka, *Chem. Commun.*, 2004, 2342-2343.
41. Y. Lu, F. Hasegawa, T. Goto, S. Ohkuma, S. Fukuhara, Y. Kawazu, K. Totani, T. Yamashita and T. Watanabe, *J. Mater. Chem.*, 2004, 14, 75-80.
42. S. J. K. Pond, M. Rumi, M. D. Levin, T. C. Parker, D. Beljonne, M. W. Day, J.-L. Brédas, S. R. Marder and J. W. Perry, *J. Phys. Chem. A*, 2002, 106, 11470-11480.
43. O. Mongin, L. Porrès, M. Charlot, C. Katan and M. Blanchard-Desce, *Chem. Eur. J.*, 2007, 13, 1481-1498.
44. Y. Wang, G. S. He, P. N. Prasad and T. Goodson, *J. Am. Chem. Soc.*, 2005, 127, 10128-10129.
45. Y. Wang, M. I. Ranasinghe and T. Goodson, *J. Am. Chem. Soc.*, 2003, 125, 9562-9563.
46. E. Zojer, D. Beljonne, P. Pacher and J.-L. Brédas, *Chem. Eur. J.*, 2004, 10, 2668-2680.
47. H. M. Kim, Y. O. Lee, C. S. Lim, J. S. Kim and B. R. Cho, *J. Org. Chem.*, 2008, 73, 5127-5130.
48. Y. Wan, L. Yan, Z. Zhao, X. Ma, Q. Guo, M. Jia, P. Lu, G. Ramos-Ortiz, J. L. Maldonado, M. Rodríguez and A. Xia, *J. Phys. Chem. B*, 2010, 114, 11737-11745.
49. H. Maeda, T. Maeda, K. Mizuno, K. Fujimoto, H. Shimizu and M. Inouye, *Chem. Eur. J.*, 2006, 12, 824-831.
50. G. Venkataramana and S. Sankararaman, *Eur. J. Org. Chem.*, 2005, 2005, 4162-4166.
51. S.-W. Yang, A. Elangovan, K.-C. Hwang and T.-I. Ho, *J. Phys. Chem. B*, 2005, 109, 16628-16635.
52. H. Shimizu, K. Fujimoto, M. Furusyo, H. Maeda, Y. Nanai, K. Mizuno and M. Inouye, *J. Org. Chem.*, 2007, 72, 1530-1533.
53. S. Leroy-Lhez and F. Fages, *Eur. J. Org. Chem.*, 2005, 2005, 2684-2688.
54. G. Klaerner and R. D. Miller, *Macromolecules*, 1998, 31, 2007-2009.
55. S. A. Jenekhe and J. A. Osaheni, *Science*, 1994, 265, 765-768.
56. A. M. Reddy, V. R. Gopal and V. J. Rao, *Radiat. Phys. Chem.*, 1997, 49, 119-125.
57. N. S. M. M. Drobizhev, A. Rebane, G. de la Torre, T. Torres, *J. Phys. Chem. C*, 2008, 112, 848-859.
58. K. Ohta, S. Yamada, K. Kamada, A. D. Slepkov, F. A. Hegmann, R. R. Tykwinski, L. D. Shirtcliff, M. M. Haley, P. Sałek, F. Gel'mukhanov and H. Ågren, *J. Phys. Chem. A*, 2010, 115, 105-117.
59. K. Susumu, J. A. N. Fisher, J. Zheng, D. N. Beratan, A. G. Yodh and M. J. Therien, *J. Phys. Chem. A*, 2011, 115, 5525-5539.
60. J. M. Hales, M. Cozzuol, T. E. O. Screen, H. L. Anderson and J. W. Perry, *Opt. Express*, 2009, 17, 18478-18488.
61. A. Rebane, M. Drobizhev, N. S. Makarov, E. Beuerman, J. E. Haley, D. M. Krein, A. R. Burke, J. L. Flikkema and T. M. Cooper, *J. Phys. Chem. A*, 2011, 115, 4255-4262.
62. F. Terenziani, C. Katan, E. Badaeva, S. Tretiak and M. Blanchard-Desce, *Adv. Mater.*, 2008, 20, 4641-4678.
63. R. Chinchilla and C. Nájera, *Chem. Rev.*, 2007, 107, 874-922.
64. K. Sonogashira, Y. Tohda and N. Hagihara, *Tetrahedron Lett.*, 1975, 16, 4467-4470.
65. S. Takahashi, Y. Kuroyama and K. Sonogashira, *Synthesis*, 1980, 627.
66. S. R. Meech and D. Phillips, *J. Photochem.*, 1983, 23, 193-217.

67. T. V. Duncan, I. V. Rubtsov, H. T. Uyeda and M. J. Therien, *J. Am. Chem. Soc.*, 2004, 126, 9474-9475.
68. N. S. Makarov, J. Campo, J. M. Hales and J. W. Perry, *Opt. Mater. Express*, 2011, 1, 551-563.
69. N. S. Makarov, M. Drobizhev and A. Rebane, *Opt. Express*, 2008, 16, 4029-4047.
70. M. J. Frisch, G. W. Trucks, H. B. Schlegel, G. E. Scuseria, M. A. Robb, J. R. Cheeseman, J. A. Montgomery Jr., T. Vreven, K. N. Kudin, J. C. Burant, J. M. Millam, S. S. Iyengar, J. Tomasi, V. Barone, B. Mennucci, M. Cossi, G. Scalmani, N. Rega, G. A. Petersson, H. Nakatsuji, M. Hada, M. Ehara, K. Toyota, R. Fukuda, J. Hasegawa, M. Ishida, T. Nakajima, Y. Honda, O. Kitao, H. Nakai, M. Klene, X. Li, J. E. Knox, H. P. Hratchian, J. B. Cross, V. Bakken, C. Adamo, J. Jaramillo, R. Gomperts, R. E. Stratmann, O. Yazyev, A. J. Austin, R. Cammi, C. Pomelli, J. W. Ochterski, P. Y. Ayala, K. Morokuma, G. A. Voth, P. Salvador, J. J. Dannenberg, V. G. Zakrzewski, S. Dapprich, A. D. Daniels, M. C. Strain, O. Farkas, D. K. Malick, A. D. Rabuck, K. Raghavachari, J. B. Foresman, J. V. Ortiz, Q. Cui, A. G. Baboul, S. Clifford, J. Cioslowski, B. B. Stefanov, G. Liu, A. Liashenko, P. Piskorz, I. Komaromi, R. L. Martin, D. J. Fox, T. Keith, M. A. Al-Laham, C. Y. Peng, A. Nanayakkara, M. Challacombe, P. M. W. Gill, B. Johnson, W. Chen, M. W. Wong, C. Gonzalez and J. A. Pople, Gaussian Inc., Wallingford CT, A.02 edn., 2009.
71. M. Lundberg and P. E. M. Siegbahn, *J. Phys. Chem. B*, 2005, 109, 10513-10520.
72. T. Yanai, D. P. Tew and N. C. Handy, *Chem. Phys. Lett.*, 2004, 393, 51-57.
73. P. V. Vyas, A. K. Bhatt, G. Ramachandraiah and A. V. Bedekar, *Tetrahedron Lett.*, 2003, 44, 4085-4088.
74. J. Grimshaw and J. Trocha-Grimshaw, *J. Chem. Soc., Perkin Trans. 1*, 1972, 0, 1622-1623.
75. S. Bernhardt, M. Kastler, V. Enkelmann, M. Baumgarten and K. Müllen, *Chem. Eur. J.*, 2006, 12, 6117-6128.
76. I. I. Perepichka, I. F. Perepichka, M. R. Bryce and L.-O. Palsson, *Chem. Commun.*, 2005, 3397-3399.
77. J. Yang, C. Jiang, Y. Zhang, R. Yang, W. Yang, Q. Hou and Y. Cao, *Macromolecules*, 2004, 37, 1211-1218.
78. W. Deng, Y. Wang, C. Zhang, L. Liu and Q.-X. Guo, *Chin. Chem. Lett.*, 2006, 17, 313-316.
79. C. Reichardt and T. Welton, *Solvents and solvent effects in organic chemistry*, Wiley-VCH, Weinheim, Germany, 4th, updated and enl. edn., 2011.
80. P. Suppan, *J. Photochem. Photobiol. A*, 1990, 50, 293-330.
81. Z. Zhao, X. Xu, H. Wang, P. Lu, G. Yu and Y. Liu, *J. Org. Chem.*, 2007, 73, 594-602.
82. V. R. Gopal, A. M. Reddy and V. J. Rao, *J. Org. Chem.*, 1995, 60, 7966-7973.
83. M. Drobizhev, N. S. Makarov, T. Hughes and A. Rebane, *J. Phys. Chem. B*, 2007, 111, 14051-14054.
84. R. Nifosì and Y. Luo, *J. Phys. Chem. B*, 2007, 111, 14043-14050.
85. M. Drobizhev, S. Tillo, N. S. Makarov, T. E. Hughes and A. Rebane, *J. Phys. Chem. B*, 2009, 113, 855-859.
86. Y. Niko, H. Moritomo, H. Sugihara, Y. Suzuki, J. Kawamata and G.-I. Konishi, *J. Mater. Chem. B*, 2015, 3, 184-190.
87. M. Rumi, S. J. K. Pond, T. Meyer-Friedrichsen, Q. Zhang, M. Bishop, Y. Zhang, S. Barlow, S. R. Marder and J. W. Perry, *J. Phys. Chem. C*, 2008, 112, 8061-8071.
88. C. Katan, F. Terenziani, O. Mongin, M. H. V. Werts, L. Porrès, T. Pons, J. Mertz, S. Tretiak and M. Blanchard-Desce, *J. Phys. Chem. A*, 2005, 109, 3024-3037.

GRAPHICAL ABSTRACT

A series of Fluorenylethynylpyrene derivatives with strong Two-Photon Absorption cross-sections (≈250-2500 GM) and good fluorescence quantum yields (Φ_{fl} = 0.55-0.98) make these dyes as good Two-Photon brighteners.